HHS Public Access

Author manuscript

Nat Cancer. Author manuscript; available in PMC 2024 July 01.

Published in final edited form as:

Nat Cancer. 2023 July ; 4(7): 1001–1015. doi:10.1038/s43018-023-00573-4.

c-Kit signaling potentiates CAR T-cell efficacy in solid tumors by CD28- and IL-2–independent costimulation

Yuquan Xiong[1], **Meriem Taleb**[1], **Kyohei Misawa**[1], **Zhaohua Hou**[1], **Srijita Banerjee**[1], **Alfredo Amador-Molina**[1], **David R. Jones**[1], **Navin K. Chintala**[1], **Prasad S. Adusumilli**[1,2,*]

[1]Thoracic Service, Department of Surgery, Memorial Sloan Kettering Cancer Center, New York, NY, USA

[2]Center for Cell Engineering, Memorial Sloan Kettering Cancer Center, New York, NY, USA

Abstract

The limited efficacy of chimeric antigen receptor (CAR) T-cell therapy for solid tumors necessitates engineering strategies that promote functional persistence in an immunosuppressive environment. Herein, we exploit c-Kit signaling, a physiological pathway associated with stemness in hematopoietic progenitor cells (T cells lose expression of c-Kit during differentiation). CAR T cells with intracellular expression—but no cell-surface receptor expression—of the c-Kit D816V mutation (KITv) have upregulated STAT phosphorylation, antigen-activation-dependent proliferation, CD28- and IL-2–independent and IFN-γ–mediated costimulation, augmenting the cytotoxicity of first-generation CAR T cells. This translates to enhanced survival, including in TGF-β–rich and low-antigen-expressing solid tumor models. KITv CAR T cells have equivalent or better *in vivo* efficacy than second-generation CAR T cells and are susceptible to tyrosine kinase inhibitors (safety switch). When combined with CD28 costimulation, KITv costimulation functions as a third signal, enhancing efficacy and providing a potent approach to treat solid tumors.

Whereas T cells redirected to target cancer cells by the use of genetically engineered chimeric antigen receptors (CARs) generate complete responses in hematological malignancies, they have had limited success in solid tumors, necessitating approaches that potentiate antitumor efficacy without overt toxicity. CARs are synthetic receptors that bind to cancer-cell-surface antigens via an extracellular single-chain variable fragment (scFv), which results in initiation of an intracellular T-cell activation domain (signal 1) and, thereby, cytotoxicity.[1] To improve proliferation of antigen-activated CAR T cells, costimulatory domains (signal 2; most commonly, CD28 and 4-1BB) have been incorporated

[*]**Correspondence:** Prasad S. Adusumilli, MD, FACS, Attending and Deputy Chief, Thoracic Service, Vice Chair, Department of Surgery, Co-Director, Mesothelioma Program, Memorial Sloan Kettering Cancer Center, 1275 York Avenue, New York, NY 10065, Phone: (212) 639-8093; Fax: (646) 422-2340, adusumip@mskcc.org.

Author Contributions Statement

P.S.A. is responsible for the original concept of the study. P.S.A. and Y.X. designed and guided the studies. Y.X., M.T., K.M., S.B., N.K.C., Z.H., A.A.-M., and P.S.A. contributed to the study methodology and investigations. Y.X., M.T., N.K.C., and P.S.A. interpreted results and performed study analysis. Y.X. and P.S.A. wrote the original draft of the manuscript. Y.X., M.T., N.K.C., and P.S.A. performed scientific editing and revision. Y.X., M.T., K.M., S.B., N.K.C., Z.H., A.A.M., D.R.J., and P.S.A. reviewed the manuscript draft. P.S.A. acquired funding.

Code availability. No custom code was generated in the course of this study.

into CAR T cell products.[2] However, signal 2 alone is inadequate to achieve functional persistence of second-generation CAR T cells in an immunosuppressive, solid tumor microenvironment.[3–5] To overcome the hurdles posed by solid tumors, efforts have been made to provide "super stimulation" via exogenously administered cytokines (IL-2 or IFN-γ) or a combination of two costimulatory domains (CD28 and 4-1BB); however, such efforts have resulted in dysfunctional CAR T cells and/or higher cytokine-induced toxicity or checkpoint inhibition.[6–8] Transcriptome analysis of CAR T cells from clinical trials showed that STAT3 signaling was associated with better efficacy.[9] To enhance STAT3 and STAT5 signaling, second-generation CAR T cells have been engineered with IL-4, IL-23, IL-2R, and IL-7R domains[10–13] to promote targeted and "sustained" stimulation (signal 3).[14, 15] The identification of a signaling domain that can function as either signal 2 or signal 3 and provide CD28- and IL-2–independent sustained costimulation (thus resulting in less T-cell exhaustion) could potentiate successful solid tumor cell therapy.

KIT (c-Kit, CD117, stem cell factor receptor), a type III receptor tyrosine kinase expressed in stem cell populations, is essential for the development of erythrocytes, germ cells, melanocytes, and mast cells, and plays a crucial role in cell proliferation and differentiation.[16] Whereas most hematopoietic progenitor cells—including Pro-T1, Pro-T2, Pre-T1, and Pre-T2—express CD117, T cells lose c-Kit expression as they mature.[17–19] *c-Kit* transcript has been detected in activated T cells without cell-surface c-Kit expression.[20, 21] Dysregulation of c-Kit signaling or gain-of-function mutations combined with other genetic or epigenetic changes have been correlated with tumorigenesis.[22–24] The D816V mutation in the activating loop of c-Kit, first observed in mast cells in systemic mastocytosis,[25–30] constitutively triggers the activation of c-Kit signaling without the need for stem cell factor ligation to the extracellular domain of c-Kit.[31] Constitutive phosphorylation of STAT1, STAT3, and STAT5 have been observed in *c-Kit D816V* cells.[32–34] However, the relatively stable course of disease in most patients with systemic mastocytosis and the association between c-Kit and indolent tumor suggests that other genetic and epigenetic factors—besides a mutation in *c-Kit*—play a larger role in outcomes.[22, 30] c-Kit D816V transgenic mice exhibited clinical signs of mastocytosis 12 to 18 months after transgenesis and with only 30% penetrance.[22] c-Kit also acts as an intrinsic tumor suppressor via its pro-death activity.[35] Indeed, in $CD8^+$ T cells derived from human umbilical cord blood mononuclear cells, c-Kit expression was associated with lower proliferation and differentiation and higher sensitivity to pro-apoptotic stimuli.[21] *c-KIT D816V* mutation plays a well-known functional role in progenitor cells and has a lack of known oncogenicity in T cells. We therefore hypothesized that an engineered intracellular fragment of c-Kit D816V (KITv) in a CAR could act as signal 2 or signal 3, promoting STAT3 and STAT5 signaling in CAR T cells and achieving the sustained stimulation required for functional persistence of CAR T cells in solid tumors.

Herein, we demonstrate, using multiple solid tumor models, that KITv-costimulated CAR T cells have comparable antitumor efficacy to CD28-costimulated CAR T cells. The combination of KITv and CD28 costimulation is noncomplementary and enhances CAR T-cell potency, including in tumors with TGF-β–induced immunosuppression or low antigen expression. The use of KITv CAR T cells to treat solid tumors is further supported by their IFN-γ–mediated cytotoxicity, antigen-activation–dependent proliferation, absence of

toxicity, low PD-1 expression, and high sensitivity to clinically available tyrosine kinase inhibitors (safety switch).

Results

KITv CAR T cells exhibit constitutive STAT phosphorylation.

To investigate whether D816V-mutated c-Kit (KITv CAR) can generate optimal CAR T-cell activity, we used retroviral vector–based, mesothelin (MSLN) antigen–targeted, first-generation CARs; Mz and second-generation CARs; M28z containing an scFv targeting MSLN; and P28z targeting prostate-specific membrane antigen (PSMA). M28z CAR T cells have already been translated to phase I and II clinical trials by our group (NCT02414269, NCT02792114, and NCT04577326).[36–40] The CARs were then N-terminally linked to an intracellular domain of D816V-mutated c-Kit via a 2A peptide sequence (Mz, Mz-KITv, M28z, M28z-KITv, P28z). We generated an additional, control CAR construct with an intracellular domain of c-Kit (KITwt; M28z-KITwt) (Fig. 1a). A c-myc-tag or ΔLNGFR was included for flow cytometric detection of CARs. All the CARs were efficiently expressed on the cell surface of multiple donor T cells (Fig. 1b). The phosphorylated KIT was detected in KITv-expressing CAR T cells but not in KITwt-expressing control CAR T cells (Fig. 1c). When co-cultured with $MSLN^+$ targets (Fig. 1d), both first- and second-generation Mz-KITv and M28z-KITv CAR T cells had significantly higher T-cell–mediated killing in 4- and 18-hour cytotoxicity assays, compared with M28z, Mz, and P28z CAR T cells (Fig. 1e). However, in response to *in vitro* sequential antigen stimulation with $MSLN^+$ tumor cells, the accumulation of M28z and M28z-KITv CAR T cells was higher than that of Mz and Mz-KITv CAR T cells (Fig. 1f). After coculture with $MSLN^+$ tumor cells for 24 hours, M28z-KITv CAR T cells secreted IFN-γ at a 4.2-fold higher level than M28z CAR T cells but secreted IL-2 at a significantly lower level. Mz-KITv CAR T cells also secreted IFN-γ at a 2.6-fold higher level than M28z CAR T cells but secreted both TNF-α and IL-2 at significantly lower levels (Fig. 1g). The higher cytotoxicity and lower proliferation capability of KITv CAR T cells can be explained by the fact that IFN-γ–producing $CD8^+$ T cells display a higher cytotoxic potential,[41, 42] and IL-2 is a key factor in driving proliferation of activated CAR T cells.[43] Despite activation and potent antigen-dependent cytotoxicity—perhaps due to low levels of IL-2 secretion—KITv CAR T cells, including M28z-KITv CAR T cells, exhibited a lower proportion of $PD1^+$ CD4 and $PD1^+$ CD8 T cells, compared with M28z CAR T cells (Extended Data Fig. 1a) and after both initial and repeat antigen stimulation (Extended Data Fig. 1b). These observations support a CD28-IL2–independent, IFN-γ–mediated cytotoxicity in KITv CAR T cells. Consistent with the functions of c-Kit D816V signaling, both CD4 and CD8 KITv CAR T cells had higher constitutive activation of STAT1, STAT3, and STAT5, compared with M28z CAR T cells (Fig. 1h). Further, in the presence of STAT3/5 inhibitor, the antigen-specific toxicity of M28z-KITv CAR T cells was inhibited in a dose-dependent manner, supporting the role of STAT signaling in the induction of cytotoxicity of KITv CAR T cells (Fig. 1i). c-Kit is expressed on the majority of hematopoietic stem cells—it plays a key role in stemness of hematopoietic stem cells, such as the ability to proliferate and differentiate,[44] but it is not expressed on mature T cells. Consistent with c-Kit signaling, KITv CAR T cells maintained the population of less-differentiated memory $CD8^+CD45RA^+CD62L^+$ T cells, which were

significantly more abundant than M28z CAR T cells (Fig. 1j,k).[45, 46] Overall, these data highlight the activation of STAT signaling in KITv CAR T cells, as well as their potent antitumor activity (compared with second-generation M28z CAR T cells), albeit with a low proliferation capacity. When combined with CD28 costimulation, KITv CAR T cells exhibit enhanced potency and proliferation.

KITv enhances the antitumor efficacy in solid tumor models.

To determine the *in vivo* functionality of KITv CAR T cells, we first investigated KITv CAR T cells in an orthotopic model of malignant pleural mesothelioma. NSG mice engrafted with intrapleural MSTO-M cells expressing high levels of MSLN were treated with a single intrapleural dose of 5×10^4 CAR T cells, ten days after tumor engraftment (Fig. 2a). Progression and regression of tumor burden in control and MSLN-targeted CAR T cells was observed by tumor bioluminescence imaging (BLI) (Fig. 2b). In this aggressive solid tumor model (i.e., all mice died within 20 days[36, 37]), mice treated with Mz-KITv CAR T cells had longer survival than mice treated with Mz CAR T cells but shorter survival than mice treated with M28z CAR T cells (median survival, 52 vs. 30 vs. 114 days); survival was not significantly different between mice treated with M28z-KITv T cells and mice treated with M28z CAR T cells (median survival, 106 vs. 114 days) (Fig. 2c).

To confirm the reproducibility of our findings of *in vivo* efficacy in solid tumors, we next investigated KITv CAR T cells in a lung cancer xenograft model (Fig. 2d–g). We engrafted A549-M non-small cell lung cancer cells expressing MSLN (Fig. 2e) in NOD-SCID-Il2rg$^{-/-}$ (NSG) mice by tail vein injection and treated them with a single, low dose of 1×10^5 CAR T cells administered 20 days after tumor engraftment (Fig. 2d). M28z-KITv CAR T cells and Mz-KITv CAR T cells both had stronger antitumor activity and were associated with significantly longer survival, compared with M28z CAR T cells and Mz CAR T cells (median survival, 103 vs. 83; 70 vs. 42 days) (Fig. 2g). M28z-KITv CAR T cells achieved better survival than Mz-KITv CAR T cells. In line with this observation, both mice treated with M28z-KITv T cells and mice treated with Mz-KITv CAR T cells had >20-fold higher plasma IFN-γ and IL-10 levels at day 10 after CAR T-cell treatment, compared with mice treated with M28z CAR T cells; levels of IL-2, IL-6, and TNF-α were not significantly different between groups (Fig. 2h). To investigate functional persistence, mice with tumor eradication after treatment with M28z-KITv CAR T cells (confirmed by serial BLI) were rechallenged with A549-M cells 123 days after initial CAR T-cell treatment. These mice exhibited resistance to tumor establishment, with a rapid decline in tumor bioluminescence, indicating long-term functional persistence of M28z-KITv CAR T cells (Extended Data Fig. 2). Thus, KITv CAR T cells have potent *in vivo* antitumor efficacy and functional persistence, compared with second-generation M28z CAR T cells, without any observed toxicity.

KITv potentiates CAR T cells in a TGF-β–rich solid tumors.

The benefit in survival associated with KITv CAR T cells was different between the mesothelioma model and the non-small cell lung cancer model, prompting us to explore the differences. Whereas both A549-M and MSTO-M cells express high levels of antigen, 60% of A549-M cells express TGF-β, compared with only 3% of MSTO-M cells (Fig. 3a). TGF-

β is one of the main immunosuppressive cytokines in solid tumors, and IFN-γ–potentiated T cells can achieve higher cytotoxicity in a TGF-β–rich tumor microenvironment.[47, 48] To investigate the exciting potential of KITv CAR T cells in a TGF-β–rich tumor microenvironment, we transduced MSTO-M cells to overexpress TGF-β (MSTOM-TGFβ) and confirmed the high expression levels of TGF-β *in vitro* and *in vivo* (Fig. 3a,b); these levels are comparable to the levels seen in patients with mesothelioma and lung cancer.[49–53] To confirm that IFN-γ–signaling is the key mechanistic pathway of KITv CAR T-cell potency, we generated M28z-KITv CAR T IFN-γ knock-out (KO) cells using CRISPR-Cas9–based gene editing; knock-out efficiency was confirmed by flow cytometry (Fig. 3c). *In vivo* (Fig. 3d–f), MSTOM-TGFβ tumors were more aggressive than MSTO-M tumors (median survival of mice, 10 vs. 18 days). M28z CAR T cells barely controlled MSTOM-TGFβ tumor growth, whereas a single dose of 1×10^5 KITv CAR T cells eliminated tumors in half of treated mice (Fig. 3e). Treatment with KITv CAR T cells (M28z-KITv and Mz-KITv) was associated with longer survival (Fig. 3f) than treatment with M28z CAR T cells (median survival, 89 vs. undefined vs. 55 days). Importantly, M28z-KITv IFN-γ KO CAR T-cell–treated mice did not control tumor progression, resulting in similar survival to control P28z-treated mice (median survival 7 vs. 10 days) (Fig. 3f). Together, these observations underscore the potential of KITv CAR T cells in solid tumors with an immunosuppressive microenvironment and highlight the predominant role of the IFN-γ–signaling pathway in triggering the therapeutic activity of KITv CAR T cells.

KITv CAR T cells are effective against low-antigen targets.

In addition to the predominant IFN-γ–signaling pathway, higher levels of CD3ζ and ERK phosphorylation were observed in KITv CAR T cells (Fig. 4a) following antigen stimulation that could enhance the response against targets with low-antigen expression;[54] this is a known hurdle in solid tumor adoptive cell therapy. *In vitro*, KITv CAR T cells efficiently killed low-MSLN-expressing A549 (Fig. 4b) cells, whereas M28z CAR T cells had no cytotoxicity even at high effector:target (E:T) ratios (Fig. 4c). This observation suggested that KITv CAR T cells have the potential to overcome the barrier of antigen heterogeneity in solid tumors. To further confirm this potential *in vivo*, mice established with low-MSLN-expressing A549 tumors were treated with a single dose of 5×10^5 CAR T cells (Fig. 4d). Mice treated with M28z-KITv or Mz-KITv CAR T cells had longer survival than mice treated with M28z CAR T cells (median survival, 98 vs. 61 vs. 56 days). Mice treated with M28z-KITv CAR T cells had better control of tumor burden (Fig 4e) and longer survival than mice treated with Mz-KITv CAR T cells (median survival, 98 vs 61 days) (Fig. 4e,f). Mice treated with M28z-KITv CAR T cells had significantly higher levels of plasma IFN-γ than mice treated with M28z CAR T cells (Fig. 4g). These results were reproduced in a tumor model established with orthotopic pleural mesothelioma with MSTO-M^{low} cells. We did not observe any on-target, off-tumor toxicity against mouse MSLN expressed in the pleura, pericardium and peritoneum (i.e., our MSLN CAR scFv cross-reacted with mouse MSLN, albeit at a higher threshold[55]). To confirm that treatment with KITv CAR T cells with reactivity against low-antigen targets does not result in toxicity against normal mesothelial cells, we first performed an *in vitro* cytotoxicity assay against high-antigen–expressing MSTO-M cells, low-antigen–expressing MSTO-M^{low} cells, and human mesothelial cells (MET-5A) expressing very low levels of MSLN (Fig. 5a,b). No

cytotoxicity was observed against mesothelial cells expressing very low levels of MSLN. *In vivo*, in mice established with orthotopic mesothelioma with MSTO-M^{low} cells (Fig. 5c), both M28z-KITv and Mz-KITv CAR T cells were associated with significantly longer survival, compared with M28z CAR T cells (Fig. 5d). In addition to demonstrating potent antitumor efficacy in an immunosuppressive microenvironment, these results underscore the efficacy of KITv CAR T cells in heterogenous-antigen-expressing tumors, a clear advantage over current, second-generation, CD28-costimulated CAR T cells; CD28 CAR T cells perform better than 4-1BB costimulated CAR T cells[2] against low-antigen targets.

KITv enhances antitumor activity of PSMA-targeted CAR T cells.

To further validate the generalizability of the results observed with KITv CAR T cells, we tested CARs targeting PSMA, which is another solid tumor cell-surface antigen. We generated retroviral CAR constructs, P28z-KITv and Pz-KITv, to target PSMA (Fig. 6a,b) as well as PSMA-overexpressing A549-P cells and prostate cancer PC3-P cells (Fig. 6c). Similar to our observations from the A549-M tumor model, in the A549-P tumor model (Fig. 6d) both P28z-KITv and Pz-KITv CAR T cells had stronger antitumor activity and were associated with significantly longer survival, compared with P28z CAR T cells (median survival, 112 vs. 95 vs. 79 days) (Fig. 6e,f). At 10 days after CAR T-cell treatment, A549-P tumor–bearing mice treated with P28z-KITv CAR T cells and those treated with Pz-KITv CAR T cells had significantly higher levels of plasma IFN-γ and IL-10 and lower levels of plasma IL-2 than mice treated with P28z CAR T cells (Fig. 6g). Furthermore, in a prostate cancer PC3-P tumor model, both P28z-KITv and Pz-KITv CAR T cells had stronger antitumor activity and were associated with significantly longer survival than P28z CAR T cells (median survival, undefined vs. undefined vs. 83 days) (Fig. 6h–j). These results validate the enhanced antitumor efficacy of KITv CAR T cells against targets expressing different antigens relevant to solid tumors.

KITv CAR T cells have a unique signaling profile.

We performed RNA-seq analysis to elucidate the molecular basis underlying the enhanced functions of KITv CAR T cells. We mapped the top 50 differentially expressed genes between M28z and M28z KITv CAR T cells before stimulation (Extended Data Fig. 3a–e); among those with elevated expression profiles were granulocyte differentiation genes, including *CSFR3*, *CBFA2T3*, and *S100A9* (Extended Data Fig. 3a). Recent studies have shown that the expression of transcription factors plays an important role in regulating CAR T-cell function in solid tumors[56, 57]; therefore, we analyzed transcription factors and discovered that the AP-1-bZIP and bZIP-IRF binding motifs were the most significantly enriched in M28z-KITv T cells—this was most pronounced in *JUNB*, *JDP2*, *FOSL1*, *FOSL2*, *BATF*, *BATF2*, *BATF3*, *ATF3*, *CEBPB*, *CEBPD*, *IRF7*, and *IRF8* (Extended Data Fig. 3b). Of note, many of these transcription factors are the downstream targets of STAT signaling.[58] Interestingly, recent studies have shown that overexpression of BATF family members may counter exhaustion and therefore lead to stronger antitumor responses of CAR T cells.[59] Consistent with higher activation of STATs in KITv CAR T cells (Fig. 1d), gene set enrichment analysis showed a significant enrichment of JAK-STAT3 and IL2-STAT5 gene sets in M28z-KITv CAR T cells, compared with M28z CAR T cells (Extended Data Fig. 3c). Consistent with increased secretion of IFN-γ (Fig. 2d) after antigen stimulation,

genes within the IFN-γ and IFN-α gene sets (Extended Data Fig. 3d) were enriched in M28z-KITv CAR T cells, compared with M28z CAR T cells, and many of the top 50 differentially expressed genes were interferon-induced genes, including *IFIT1*, *IFTI3*, *IFI6*, *CXCL9*, *CXCL10*, and *MX1* (Extended Data Fig. 3d). Overall, the elevated signaling of STATs and the upregulation of interferon pathway genes (Extended Data Fig. 3e) are consistent with the enhanced antitumor efficacy of KITv CAR T cells.

KITv CAR T cells are susceptible to tyrosine kinase inhibitors.

We next investigated the susceptibility of M28z-KITv CAR T cells to tyrosine kinase inhibitors—dasatinib and midostaurin. *In vitro*, although dasatinib does not affect the viability of CAR T cells (Extended Data Fig. 4a), the cytotoxicity assay in the presence of dasatinib leads to the inhibition of the antigen-specific cytotoxicity of M28z-KITv CAR T cells (Extended Data Fig. 4b). We conducted an i*n vivo* safety experiment where we injected 1×10^5 M28-KITv CAR T cells intrapleurally or intravenously to mice established with MSTO-M pleural tumor, followed by daily oral administration of dasatinib or midostaurin (50 mg/kg; twice a day) (Fig. 7a). Treatment with either dasatinib or midostaurin inhibited M28z-KITv CAR T-cell activity, and tumors progressed as indicated by the BLI signal (Fig. 7b) and survival (Fig. 7c). Moreover, in a separate cohort of mice, quantification of M28z-KITv CAR T cells in the harvested tumor by flow cytometry on day 3 CAR T-cell after administration showed lower accumulation of CAR T cells ($CD3^+$ Myc^+ cells) in mice treated with dasatinib or midostaurin than in mice that received only CAR T cells with no drug treatment (Fig. 7d). These results suggest that kinase inhibitors, such as dasatinib or midostaurin, can suppress M28z-KITv CAR T cells activity *in vivo*, highlighting their potential to be used as safety agents to treat treatment-related complications.

Discussion

Adoptive cell therapy in solid tumors is hindered by tumor microenvironment–specific obstacles that necessitate novel approaches.[60] We have demonstrated, in multiple solid tumor models, that the inclusion of c-Kit signaling in tumor-specific CAR T cells helps overcome some of these obstacles. In this study, we have made several observations that are pertinent to KITv-mediated signaling in CAR T cells: (1) c-Kit signaling was functional only after antigen activation; (2) KITv protein constitutively increased STAT phosphorylation and enhanced signal 1–induced cytotoxicity of CAR T cells; (3) when functioning as a second signal, KITv costimulation significantly enhanced the antitumor efficacy of CAR T cells, even without an increase in proliferation; (4) when added to second-generation, CD28-costimulated CAR T cells, KITv provided a robust signal 3 function; and (5) KITv costimulation is IFN-γ–mediated. The above features suggest that KITv CAR T cells are a promising candidate to specifically treat solid tumors. Furthermore, tyrosine kinase inhibitors can be employed as safety switch with reversible inhibition.

c-Kit is a well-known stem cell marker for normal hematopoietic cells, and its expression decreases as cells lose their plasticity during differentiation.[19] However, multiple investigators have observed c-Kit transcript in adult mature T cells—specifically, activated T cells—without cell-surface expression of c-Kit,[20, 21] providing a rationale for us to

investigate KITv CAR T cells. c-KIT signaling leads to the activation of many downstream signaling pathways—such as RAS/ERK, PI3-kinase, SRC, JAK/STAT, and NOTCH—that are known to induce a stemlike phenotype.[61] Not unexpectedly, KITv CAR T cells exhibited a more abundant population of $CD8^+CD45RA^+CD62L^+$ T memory cells and stronger cytotoxicity. The lack of proliferation of KITv CAR T cells in the absence of antigen activation supports the safety of our approach. Recent studies have shown that c-Kit actively triggers the cell death pathway and that c-Kit activation is associated with sensitivity to apoptosis in cord blood monocyte–derived T cells.[21, 35]

Although we predominantly compared the efficacy of M28z and M28z-KITv CAR T cells, our results with Mz CAR T cells are intriguing in that, even without CD28 costimulation, the enhanced antitumor efficacy by addition of KITv signaling as second signal is observed. These results are not limited to one experiment or one model. We have reproduced these important results in our lung cancer model, in our pleural mesothelioma model with and without high TGF-β expression, and in experiments with PSMA-targeted CAR. Furthermore, in our lung cancer model and in the experiments with PSMA-targeted CAR, Mz-KITv CAR T-cell–treated mice survived longer than M28z CAR T-cell–treated mice.

After antigen stimulation, the activity of many cytotoxic-associated genes is significantly increased in KITv CAR T cells—in particular, high levels of IFN-γ and associated signaling were observed both *in vitro* and *in vivo*. The longer survival of tumor-bearing mice after treatment with KITv CAR T cells, independent of CD28 signaling or augmented secretion of IL-2, underscores the unique advantage of these T cells for treating aggressive, immunosuppressive solid tumors. Furthermore, when combined with second-generation, CD28-costimulated CAR T cells, KITv signaling provides a noncomplementary additive effect. However, the survival advantage observed in non-small cell lung cancer and prostate cancer was not observed in pleural mesothelioma. It is worthwhile to note that the single low dose of CAR T cells (5×10^4 or 1×10^5, low E:T ratios) purposefully used in our study to mimic antigen stress in the solid tumor environment may have contributed to the lack of a significant benefit in mesothelioma. Despite lower levels of TGF-β, mesothelioma cells are known to induce high levels of PD-L1 expression,[62] including in MSTO-M cells; the robust secretion of IFN-γ by KITv CAR T cells can further upregulate PD-L1 expression. It is plausible that, although KITv CAR T cells express lower levels of PD-1 than CD28 CAR T cells, the PD-1 or PD-L1 pathway can ultimately compromise T-cell function in the presence of sustained antigen stress–induced activation.[3, 37, 38] Yet, higher levels of IFN-γ in the tumor microenvironment can augment the efficacy of immune checkpoint inhibitor agents. With this in mind, we are currently investigating the use of a PD-1 dominant negative receptor in KITv CAR T cells; the functional persistence of PD-1 dominant negative receptor CAR T cells in solid tumor models was previously described by us and translated to clinical trials.[37] However, the potency of KITv CAR T cells in TGF-β–rich tumors is a more exciting observation. Indeed, treatment with M28z CAR T cells was associated with transient regression of TGF-β–rich MSTOM-TGFβ tumors, with subsequent rapid growth of tumor; in contrast, treatment with KITv CAR T cells resulted in eradication of tumors in half of treated mice. In addition to counteracting TGF-β, KITv CAR T cells, through the robust secretion of IFN-γ, may further activate endogenous immunity in solid tumors. The stronger cytotoxic signaling resulted in efficient CAR T-cell cytotoxicity

against low-antigen-expressing tumors,[54, 63, 64] presenting an additional opportunity to treat heterogenous-antigen-expressing solid tumors.

Although c-Kit activation has been shown to be associated with oncogenic activity, expression of c-Kit D816V mutation alone is not sufficient to induce complete cell transformation,[65] and there was no evidence of such transformation in our study. IL-6, IFN-γ, and IL-10 are among the cytokines involved in cytokine release syndrome; no toxicity was observed in our *in vivo* studies. On their own, IL-6 and TNF-α have been shown to provide weak costimulation; however, together, they provided synergistic CD28- and IL-2–independent costimulation in Rag-2$^{-/-}$ or CD28 $^{-/-}$ mice.[66] This synergistic costimulation was more pronounced when IL-2 was present in our M28z-KITv CAR T cells. KITv CAR T cells are highly susceptible to tyrosine kinase inhibitors, which can serve as a safety switch in case of unexpected toxicity.[28]

In summary, we have developed a CAR construct that constitutively activates c-Kit signaling. Given the effective application of KITv to MSLN- or PSMA-targeted CAR T cells, the translational potential to treat large cohorts of patients with solid tumors is high. It is feasible to expand this approach to other CAR- and T-cell receptor–engineered T cells. Given that 4-1BBζ CAR T cells have limited efficacy against low-antigen-expressing targets, compared with CD28-costimulated CAR T cells, the addition of the KITv signaling domain can improve the targeting of solid tumors with heterogenous antigen expression by second-generation CAR T cells. Their enhanced cytotoxicity in TGF-β–rich tumors (even against low-antigen–expressing cancer cells), lack of overt toxicity, and susceptibility to clinical-grade safety agents with reversible inhibition render KITv CAR T cells highly applicable to treat solid tumors; however, the efficacy and safety of these proof-of-principle studies will be tested in upcoming trials. c-Kit has been observed to be expressed in only a small subset of CD56^{bright} natural killer cells involved in immunomodulation and, to a lesser extent, in those involved in mediating antitumor responses.[67, 68] Whether KITv can enhance the antitumor efficacy of other cell therapies, including natural killer cells, is an intriguing area of future investigation.

Online Methods

All animal studies were performed under protocol #08-01-001, which was approved by the Memorial Sloan Kettering Cancer Center Institutional Animal Care and Use Committee. All relevant animal use guidelines and ethical regulations were followed. Further information on research design is available in the Nature Research Reporting Summary linked to this article.

Cell lines and donor T cells.

Human lung cancer cells (A549 [CRM-CCL]), human pleural mesothelial cells (MeT-5A [CRL-9444), human pleural mesothelioma cells (MSTO-211H [CRL-2081]), and prostate cancer cells (PC3 [CRL-1435]) were obtained from American Type Culture Collection. As previously described,[43] A549, MSTO-211H, and PC3 cells were transduced with green fluorescent protein (GFP) and firefly luciferase (ffLuc) fusion protein to facilitate *in vivo* tracking by bioluminescence image (BLI). These cells were then transduced with human *MSLN-, PSMA*-, or *TGFβ*-gene-containing plasmids to generate MSLN (MSTO-M, A549-

M)–, PSMA (PC3-P, A549-P)–, or TGFβ (MSTOM-TGFβ)–overexpressing tumor cells. MSTO-M^{low} cancer cells expressing low levels of MSLN were produced using diluted retroviral supernatant (1:8) derived from producer cells transduced with human MSLN plasmid to generate high-MSLN-expressing MSTO-M cells. These cells were flow-sorted, passaged, and confirmed to have sustained low cell-surface expression of MSLN over several passages before using in *in vitro* and *in vivo* experiments.

Human T cells for the generation of CAR T cells were produced from peripheral blood mononuclear cells obtained as buffy coats prepared from whole blood collected by the New York Blood Center (New York, NY). All cell lines were routinely tested for mycoplasma contamination and for cell-surface expression of target antigens.

Retroviral vector construction and viral production.

MSLN-specific CARs were generated using the Myc-tag–linked MSLN-specific scFv (m912 scFv)[55] linked to the CD28H/T-CD28-CD3ζ or CD8H/T-CD3ζ domains. PSMA-specific CARs were generated using the Myc-tag–linked PSMA-specific scFv (J591 scFv)[69] linked to the CD28H/T-CD28-CD3ζ or CD28H/T-CD3ζ domains. To generate CAR constructs with the KITwt or KITv domain, the codon-optimized intracellular fragment of wild-type *KIT* gene or *KIT D816V* mutation genes were synthesized and fused to the constructs linked after a 2A sequence. The CAR sequences were inserted into the SFG γ-retroviral vector (provided by I. Riviere, Memorial Sloan Kettering Cancer Center) and then transfected into 293T H29 and 293Vec RD114 packaging cell lines to produce the retrovirus, as previously described.[37]

Generation of CAR T cells.

Blood samples from anonymous healthy donors were purchased from the New York Blood Center and were handled in accordance with all required ethical and safety procedures. Peripheral blood mononuclear cells were isolated by low-density centrifugation on Lymphoprep (Stem Cell Technology) and activated with phytohemagglutinin (2 ug/mL; Remel). Two days after isolation, peripheral blood mononuclear cells were transduced with 293VecRD114-produced retroviral particles encoding CARs by spinoculation for 1 hour at 1800 × g on plates coated with retronectin (15 μg/mL; r-Fibronectin, Takara). CAR T cells and control T cells were maintained in culture with the addition of a low concentration of IL-2 (20 IU/mL).

For M28z-KITv IFN-γ KO cells, CD3 T cells were isolated from peripheral blood mononuclear cells using the Miltenyi No-Touch T Cell Isolation Kit and stimulated with 1:1 CD3/CD28 Dynabeads (Invitrogen) in 20 U/mL of IL-2 (Miltenyi Biotech). At 48 h after initiation of T-cell activation, CD3/CD28 beads were magnetically removed, and the cells were transfected by electroporation using 1 μg of Cas9 mRNA (TriLink Biotech) and 1 μg of IFN-γ gRNA (GenScript) in a 0.2-cm cuvette in a total volume of 20 μL. The electroporation reaction was performed in a Lonza Nucleofector machine (Lonza 4DNucleofector). After electroporation, cells were diluted into culture medium and incubated at 37°C (5% CO_2) for 24 h before being spinoculated.

Western blot analysis.

Protein was extracted from cells using RIPA buffer (Thermo Fisher Scientific) supplemented with proteinase and phosphatase inhibitors (Thermo Fisher Scientific). Protein concentrations of supernatants were determined using the BCA protein assay kit (Pierce Chemical). The same amount of protein for each sample was separated on precast 4% to 15% gradient gels (Bio-Rad) by SDS-PAGE and transferred to nitrocellulose membranes (Bio-Rad). Immunoblot analysis was performed using the following antibodies: HRP Conjugate GAPDH (clone 14C10, Cell Signaling Technology), anti-c-Kit (clone D13A2, Cell Signaling Technology), anti-Phospho-c-Kit (Tyr719, Cell Signaling Technology), and goat anti-rabbit IgGHRP (Santa Cruz Biotechnology). Blots were developed with the Western blot development kit from GE Healthcare.

Flow cytometry.

For cell-surface staining, cell pellets were incubated with antibodies at room temperature for 15 min or at 4°C for 30 min. For intracellular staining, cells were fixed and permeabilized with Cytofix/CytoPerm (BD Biosciences) for 15 min at room temperature and washed with 1× PermWash (BD Biosciences). Subsequent staining was performed with 1× PermWash as the staining and wash buffer. For intracellular phosphoprotein staining, cells were fixed in 1.5% formaldehyde for 10 min at room temperature; pelleted cells were then permeabilized using ice-cold methanol at 4°C for 20 min. Cells were washed twice, and subsequent staining was performed in staining medium (phosphate buffered saline containing 1% bovine serum albumin) at 4°C for 1 h.[70] Cell pellets were additionally stained with 4′,6-diamidino-2-phenylindole (DAPI [Thermo Fisher]) or Zombie Aqua Live/Dead Discrimination dye (BioLegend) to exclude dead cells during analysis. Additional information on antibodies, clones, vendors, catalog numbers, and dilutions used in the study are provided in the Nature Research Reporting Summary linked to this article.

Data acquisition was performed on an Attune NxT flow cytometer (Thermo Fisher Scientific) and analyzed using FlowJo analysis software (Tree Star). Gating strategies used for *in vitro* and *in viv*o characterization of cellular phenotypes are provided in Extended Data Fig. 5.

T-cell functional assays.

The cytotoxicity of T cells transduced with a CAR was determined by standard ^{51}Cr-release assays and luciferase-based assays. For ^{51}Cr-release assays, MSLN^{+} tumor cells were used as target cells, as described previously.[37] For luciferase-based assays, MSLN^{+} tumor cell–expressing ffLuc-GFP served as target cells. Effector cells were cocultured in triplicate using black-walled 96-well plates at the indicated E:T ratio, with 1×10^4 target cells in a total volume of 200 μL per well. To determine maximal luciferase expression (relative light units [RLU]), target cells alone were also plated at the same cell density. At 4 or 18 h after incubation, 50 μL of luciferase substrate (Bright-Glo; Promega) was directly added to each well, and emitted light was detected using a luminescence plate reader. The percentage of lysis was determined as [(1 − (RLUsample)/(RLUmax)) × 100].

For the STAT inhibition assay, effector cells were preincubated with or without STAT3/STAT5 Dual Inhibitor (Clone SH-4–54; Calbiochem-Sigma) for 1 h before coculturing with target cells.

To analyze proliferation, CAR T cells were restimulated by irradiated tumor cells expressing MSLN every 4 days at an E:T ratio of 3:1 in triplicate. T-cell numbers were counted 4 and 8 days after initial stimulation using a hemacytometer, with plotted numbers adjusted for CAR^+ percentage as determined by flow cytometry.

Enzyme-linked immunosorbent assay.

Cell culture supernatants were collected after 24 h of culture of 2.5×10^6 tumor cells in a 24-well plate, and the release of TGF-β was measured using a specific enzyme-linked immunosorbent assay kit (R&D systems) in accordance with the manufacturer's instructions. Plasma and tumor tissues were collected from mice with a high burden of MSTO-M tumor at day 26 and from those with MSTOM-TGFβ tumors at day 18. Each supernatant was measured in duplicate. Samples were measured using the Synergy 2 Multi-Detection Microplate Reader and Gen5 software (both BioTek). After 18 h of coculturing T cells with target cells at an E:T ratio of 3:1, supernatants were collected, and cytokine levels were determined using a multiplex bead Human Cytokine Detection Kit in accordance with the manufacturer's instructions (Millipore). Blood was collected via retroorbital bleeds at day 10 of CAR T-cell treatment. Cytokine detection assays were completed in accordance with the manufacturer's specifications using a Human High Sensitivity T Cell Premixed 13-plex Cytokine Magnetic Bead Panel and the Luminex FlexMap3D system (Millipore). Cytokine concentrations were assessed using Luminex Xponent 4.2 (Millipore).

RNA extraction, transcriptome sequencing, and RNA-seq analysis.

M28z and M28z-KITv CAR T cells were unstimulated or stimulated with irradiated 3T3-MSLN for 24 h, followed by magnetic selection of $CD8^+$ cells (Miltenyi Biotec). RNA was extracted using the RNeasy Mini Kit (Qiagen) in accordance with the manufacturer's instructions.

After RiboGreen RNA quantification and quality control using an Agilent Bioanalyzer, libraries were prepared using TruSeq RNA Library Prep Kit v2 (Illumina). Sequencing was conducted on an Illumina NovaSeq 6000, generating 60 million 50-bp paired-end reads. The output data (FASTQ files) were mapped to the target genome using the STAR aligner,[71] which resolves reads across splice junctions and maps them genomically. We used the 2-pass mapping method, in which the reads are mapped twice.[72] The first mapping pass used a list of known annotated junctions from Ensemble. Novel junctions found in the first pass were then incorporated into the list of known junctions, and a second mapping pass was performed. The expression count matrix was then generated from the mapped reads using HTSeq (www-huber.embl.de/users/anders/HTSeq) and one of several possible gene model databases. The resulting raw count matrices generated by HTSeq were then subjected to normalization and differential expression analysis using the R/Bioconductor package DESeq (www-huber.embl.de/users/anders/DESeq).

In vivo experiments.

For *in vivo* experiments, 6- to 10-week-old male or female NOD-SCID-Il2rg$^{-/-}$ (NSG) mice were purchased from the Jackson Laboratory and were maintained in an institutional animal facility for at least 1 week before their use in experiments. Housing conditions are as follows: individually ventilated cages with unrestricted access to food and water, temperature ranging from 18°C to 23°C, humidity of 40% to 60%, and a cycle of 12 h of light and 12 h of dark.

For the orthotopic pleural mesothelioma mouse model, mice were anesthetized using inhaled isoflurane and oxygen, with bupivacaine administered for analgesia. Orthotopic pleural mesothelioma was established by direct intrapleural injection of 8×10^5 ffLuc-GFP MSTO-211H tumor cells in 200 μL of serum-free medium via a right thoracic incision. Ten days after establishment of tumor, mice with equivalent tumor burden were selected and sorted into cohorts by tumor bioluminescence imaging (BLI) and were treated with intrapleural administration of either 5×10^4 or 5×10^5 CAR T cells. BLI was performed using the IVIS Imaging System (PerkinElmer) with Living Image software (PerkinElmer) for the acquisition of imaging data sets. BLI signal was reported as total flux (photons per second), which represents the average of ventral and dorsal flux.

For the metastatic lung cancer model, mice were inoculated with 1×10^6 ffLuc-GFP A549 cells in 200 μL of serum-free medium by tail vein injection. Twenty days after establishment of tumor, mice with equivalent tumor burden were selected and sorted into cohorts by tumor BLI and were treated with either 5×10^4 or 5×10^5 CAR T cells administered intravenously. Tumor rechallenge experiments were performed by intraperitoneal administration of 1×10^6 ffLuc-GFP A549 cells at indicated time points.

For the metastatic prostate cancer model, mice were inoculated with 2×10^6 ffLuc-GFP PC3 cells by tail vein injection, followed, 28 days later, by a single dose of 5×10^4 CAR T cells administered intravenously.

For the safety study, mice received tyrosine kinase inhibitors (50 mg/kg dasatinib [Sigma-Aldrich] or midostaurin [Sigma-Aldrich]) prepared in a mixture of 5% DMSO, 40% PEG, 5% Tween, and 50% water after CAR T-cell infusion. Drug administration was performed by oral gavage twice daily beginning on the day of CAR T-cell infusion in the intrapleural regional delivery model or 1 day after infusion in the intravenous systemic delivery model.

To ensure mice did not exceed the high tumor burden specified in the approved animal protocol, all mice used in the experiments were monitored every 12 h for clinical signs of sickness arising from high tumor burden and were promptly euthanized upon confirmation of >20% loss of body weight accompanied by one or more of the following: change in physical appearance (i.e., with ruffled hair or unkempt appearance), lethargy or persistent recumbency, loss of a righting reflex, and/or any condition interfering with daily activity (i.e., eating, drinking, ambulation). Occasionally (<5%), mice that developed chest tumors because of missed pleural injections were excluded from the study.

Statistics and Reproducibility.

Data were analyzed using Prism software (version 9, GraphPad Software). Statistical tests included the two-tailed Student's *t* test, one-way analysis of variance (ANOVA), and two-way ANOVA, with the Sidak-Bonferroni correction used to correct for multiple comparisons when applicable. Data distribution was assumed to be normal, but this was not formally tested. For *in vivo* experiments, overall survival was depicted by Kaplan-Meier curve, and the log-rank test was used to compare differences in survival between groups. Statistical significance was defined as *p<0.05, **p<0.01, ***p<0.001, and ****p<0.0001.

Data are displayed as mean ± standard deviation. All samples meeting proper experimental conditions were included in the analysis. No statistical method was used to predetermine sample size; group sizes were determined on the basis of tumor burden determined by BLI before initiation of treatment. The experiments were not randomized; the investigators were not blinded to allocation during experiments and outcome assessment. The statistical test used and number of replications for each experiment are described in the corresponding figure legends. Further information on research design is available in the Nature Research Reporting Summary linked to this article.

Extended Data

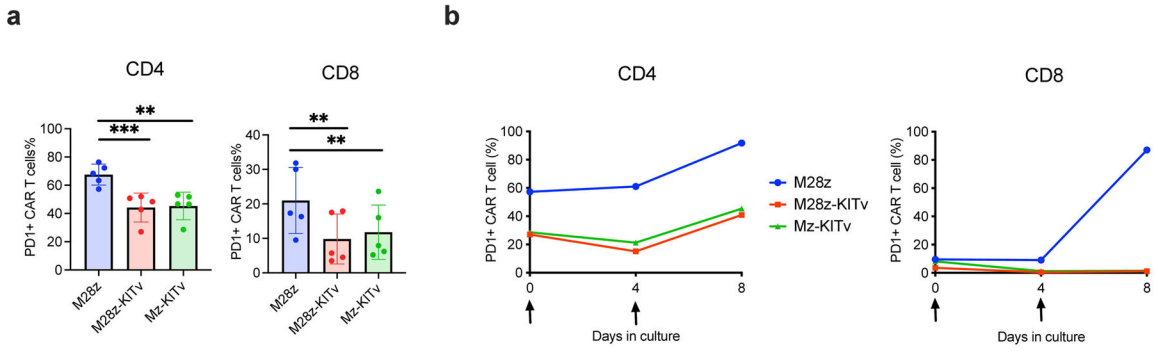

Extended Data Fig. 1. Mz-KITv and M28z-KITv CAR T cells show relatively lower levels of PD1 expression.

a, Proportion of PD1$^+$ cells in CD4 and CD8 CAR T cells after stimulation with antigen-expressing (MSLN$^+$) target cells (n=5 biological replicates; two-tailed paired *t* test **p=0.0018, M28z vs. Mz-KITv; ***p=0.0009, M28z vs. M28z-KITv in CD4 T cells; and **p=0,0013, M28z vs. M28z-KITv; **p=0.0075, M28z vs. Mz-KITv for CD8 T cells). **b**, Proportion and kinetics of PD1$^+$ cells in CD4 and CD8 CAR T cells upon stimulation with MSLN$^+$ target cells every four days, as indicated by arrows. All data shown are mean ± standard deviation and are representative of three independently repeated experiments with at least three independent donors.

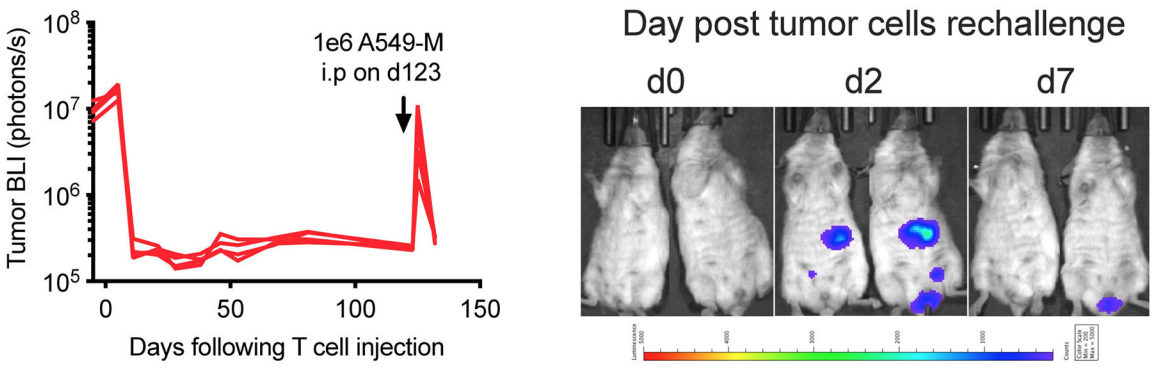

Extended Data Fig. 2: Long-term functional persistence of M28z-KITv CAR T cells.

Mice were initially established with A549-M lung cancer metastatic tumor and treated with a single dose (1×10^5) of M28z-KITv CAR T cells. After tumor eradication for 122 days, confirmed by multiple tumor bioluminescence imaging (BLI), mice were rechallenged with intraperitoneal (i.p) injection of 1×10^6 A549-M cells on day (d) 123 after initial CAR T-cell treatment, and tumor burden was monitored with BLI (n=4 mice).

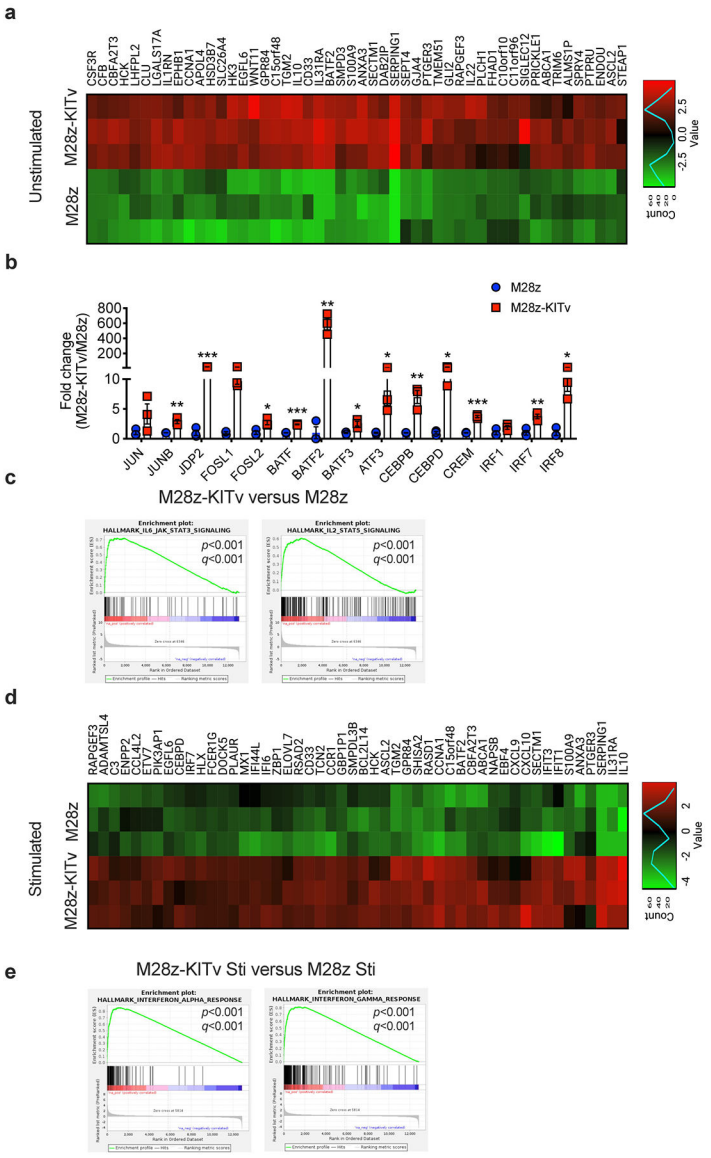

Extended Data Fig. 3: KITv CAR T cells have molecular expression profiles associated with potent cytotoxic activity.

Mesothelin (MSLN)–targeted M28z and M28z-KITv CD8$^+$ CAR T cells alone (unstimulated) or cocultured (stimulated) with MSLN-expressing 3T3-M cells for 24 hours (M28z Sti and M28z-KITv Sti) were collected, and their gene expression profiles were analyzed by RNA-seq analysis. **a**, Heat maps of the top 50 differentially expressed genes between unstimulated M28z and M28z-KITv CAR T cells. **b**, Individual gene expression of AP-1-bZip and IRF gene family members from the bulk RNA-seq analysis in unstimulated M28z (blue) and M28z-KITv (red) CAR T cells. Data are mean ± standard deviation from three samples across three different donors (*p<0.05; **p<0.01; ***p<0.001) determined by multiple t tests. **c**, Gene-set enrichment analysis, comparing the gene expression of M28z-KITv and M28Z CAR T cells for JAK-STAT3 and IL2-STAT5 gene sets. **d**, Heat maps of the top 50 differentially expressed genes between M28z Sti and M28z-KITv Sti CAR T cells. **e**, Gene-set enrichment analysis for the expression profiles of stimulated

M28z-KITv Sti compared with M28z Sti CAR T cells for IFN-α and IFN-γ gene sets. Nominal *p* values and false-discovery rate *q* values are indicated.

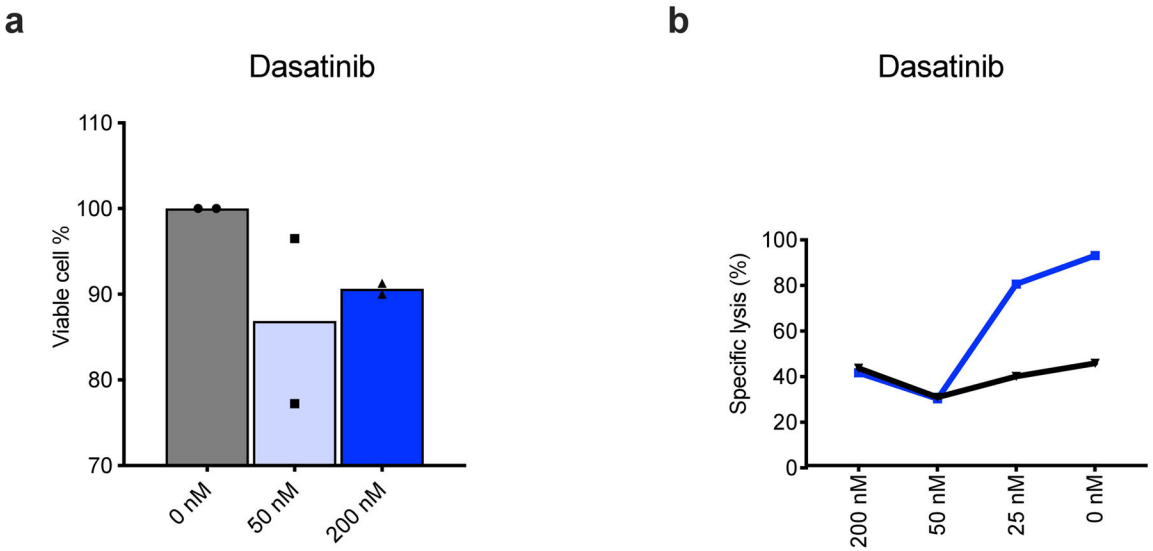

Extended Data Fig. 4: Dasatinib inhibits CAR T-cell cytotoxicity without affecting viability *in vitro*.

a, M28z-KITv CAR T cells were cultured in the presence or absence of dasatinib for 72 h. Target-cell viability was monitored by flow cytometry. The experiment was performed twice, and a representative example is shown. b, Luciferase-based cytotoxicity assay assessing M28z KITv CAR T-cell killing at 18 h when cocultured with ffLuc-expressing, mesothelin-positive target cells in the presence or absence of dasatinib (n=3 technical replicates). The experiment was performed three times, and a representative example is shown.

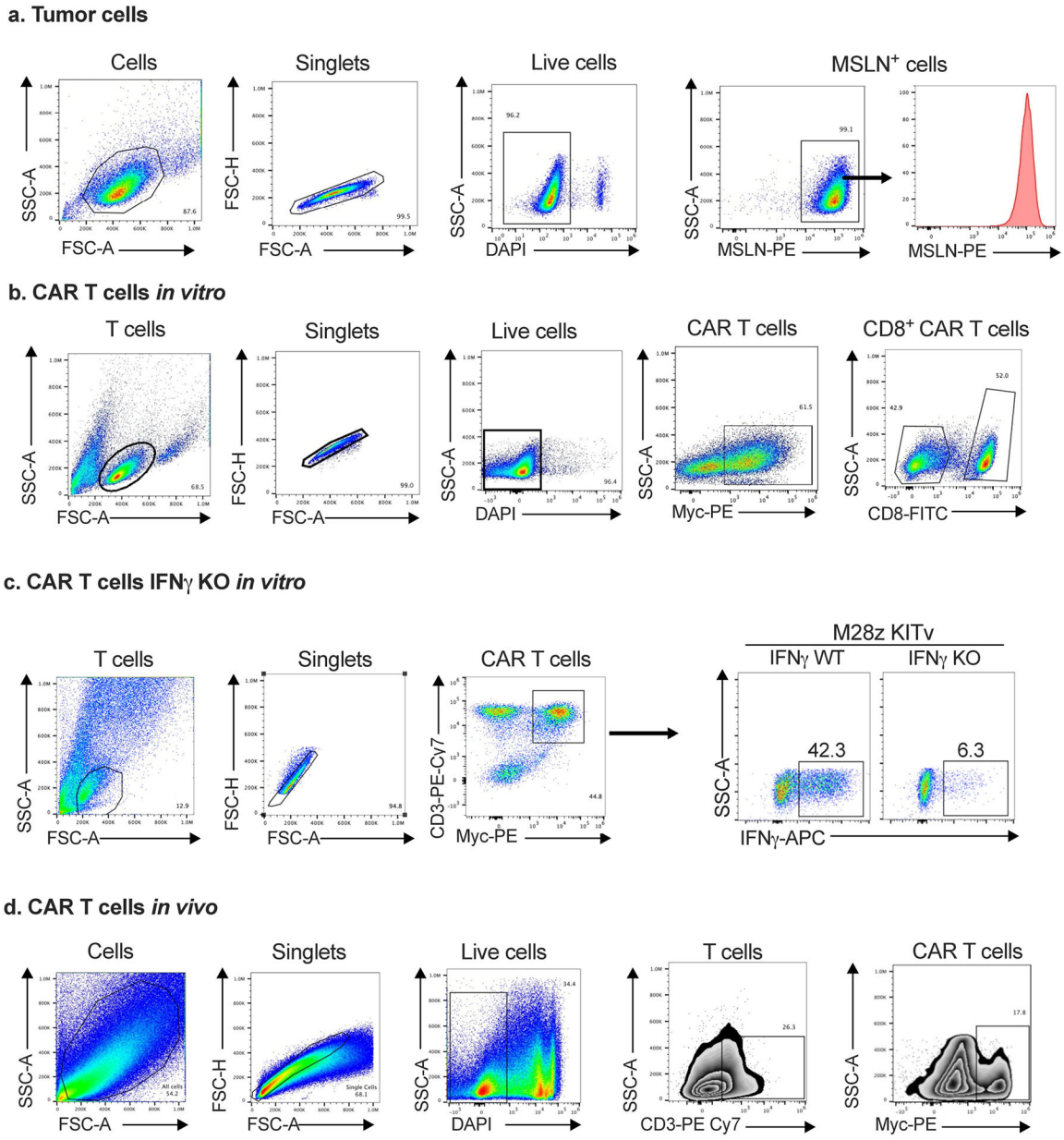

Extended Data Fig. 5: Representative gating strategy used for flow cytometry analysis.

a, Tumor cells gating strategy corresponding to data shown in Figures 1d, 2e, 4b, and 4h. **b**, CAR T cells in vitro gating strategy corresponding to data shown in Figure 1e, h, and j. **c**, IFN-γ KO CAR T cells in vitro gating strategy corresponding to data shown in Figure 3c. **d**, CAR T cells in vivo gating strategy corresponding to data shown in Figure 6d.

Acknowledgements

We thank Summer Koop and David Sewell of the Thoracic Service, Department of Surgery, Memorial Sloan Kettering Cancer Center, for excellent editorial assistance.

Funding

Dr. Adusumilli's laboratory work is supported by grants from the National Institutes of Health (grant numbers P30 CA008748, R01 CA236615-01, R01 CA235667 and U01 CA214195); the U.S. Department of Defense (grant numbers CA170630, CA180889, and CA200437); the Baker Street Foundation; the Batishwa Fellowship; the Comedy versus Cancer Foundation, the Cycle for Survival fund, the DallePezze Foundation; the Derfner Foundation; the Esophageal Cancer Education Fund; the Geoffrey Beene Foundation; the Memorial Sloan Kettering Technology Development Fund; the Miner Fund for Mesothelioma Research; the Mr. William H. Goodwin and Alice Goodwin, the Commonwealth Foundation for Cancer Research; and the Experimental Therapeutics Center of Memorial Sloan Kettering Cancer Center (P.S.A.). Dr. Adusumilli's laboratory received research support from ATARA Biotherapeutics (P.S.A.). The research support sources did not have any role in study design, collection, analysis, and interpretation of data, writing of the article, or the decision to submit the article for publication.

Competing Interests Statement

Y.X. and P.S.A. have a pending patent application on the KITv mutation as a costimulatory domain to use in T cells. P.S.A. declares research funding from ATARA Biotherapeutics and Novocure; Scientific Advisory Board Member and Consultant for Adjuvant Genomics, ATARA Biotherapeutics, Abound Bio, Bio4t2, Carisma Therapeutics, Imugene, ImmPactBio, Johnston & Johnston, Link Immunotherapeutics, Orion pharma, Outpace Bio, Pluri-biotech, Putnam associates, Verismo Therapeutics; Patents, royalties, and intellectual property on MSLN-targeted CAR and other T-cell therapies licensed to ATARA Biotherapeutics, issued patent method for detection of cancer cells using virus, and pending patent applications on PD-1 dominant negative receptor, wireless pulse-oximetry device, and an ex vivo malignant pleural effusion culture system. All other authors do not have competing interests to disclose. Memorial Sloan Kettering Cancer Center has licensed intellectual property related to MSLN-targeted CARs and T-cell therapies to ATARA Biotherapeutics and has associated financial interests.

Data availability.

RNA-seq data that support the findings of this study have been deposited in the Gene Expression Omnibus under accession code GSE229026. Source data for Fig. 1–6 and Extended Data Fig. 1–4 have been provided as Source Data files. All other data supporting the findings of this study are available from the corresponding author on reasonable request.

References

1. Sadelain M, Rivière I & Riddell S Therapeutic T cell engineering. Nature 545, 423–431 (2017). [PubMed: 28541315]
2. Cappell KM & Kochenderfer JN A comparison of chimeric antigen receptors containing CD28 versus 4–1BB costimulatory domains. Nat Rev Clin Oncol 18, 715–727 (2021). [PubMed: 34230645]
3. Grosser R, Cherkassky L, Chintala N & Adusumilli PS Combination immunotherapy with CAR T cells and checkpoint blockade for the treatment of solid tumors. Cancer Cell 36, 471–482 (2019). [PubMed: 31715131]
4. Kosti P, Maher J & Arnold JN Perspectives on chimeric antigen receptor T-cell immunotherapy for solid tumors. Front Immunol 9, 1104 (2018). [PubMed: 29872437]
5. Guedan S et al. Single residue in CD28-costimulated CAR-T cells limits long-term persistence and antitumor durability. J Clin Invest 130, 3087–3097 (2020). [PubMed: 32069268]
6. Wijewarnasuriya D, Bebernitz C, Lopez AV, Rafiq S & Brentjens RJ Excessive costimulation leads to dysfunction of adoptively transferred T cells. Cancer Immunol Res 8, 732–742 (2020). [PubMed: 32213625]
7. Drakes DJ et al. Optimization of T-cell receptor-modified T cells for cancer therapy. Cancer Immunol Res 8, 743–755 (2020). [PubMed: 32209638]
8. Zuccolotto G et al. PSMA-specific CAR-engineered T cells for prostate cancer: CD28 outperforms combined CD28-4-1BB "super-stimulation". Front Oncol 11, 708073 (2021). [PubMed: 34660275]
9. Fraietta JA et al. Determinants of response and resistance to CD19 chimeric antigen receptor (CAR) T cell therapy of chronic lymphocytic leukemia. Nat Med 24, 563–571 (2018). [PubMed: 29713085]

10. Shum T et al. Constitutive signaling from an engineered IL7 receptor promotes durable tumor elimination by tumor-redirected T cells. Cancer Discov 7, 1238–1247 (2017). [PubMed: 28830878]
11. Wang Y et al. An IL-4/21 inverted cytokine receptor improving CAR-T cell potency in immunosuppressive solid-tumor microenvironment. Front Immunol 10, 1691 (2019). [PubMed: 31379876]
12. Luo H et al. Coexpression of IL7 and CCL21 increases efficacy of CAR-T cells in solid tumors without requiring preconditioned lymphodepletion. Clin Cancer Res 26, 5494–5505 (2020). [PubMed: 32816947]
13. Ma X et al. Interleukin-23 engineering improves CAR T cell function in solid tumors. Nat Biotechnol 38, 448–459 (2020). [PubMed: 32015548]
14. Hawkins ER, D'Souza RR & Klampatsa A Armored CAR T-cells: the next chapter in T-cell cancer immunotherapy. Biologics 15, 95–105 (2021). [PubMed: 33883875]
15. Kagoya Y et al. A novel chimeric antigen receptor containing a JAK-STAT signaling domain mediates superior antitumor effects. Nat Med 24, 352–359 (2018). [PubMed: 29400710]
16. Rojas-Sutterlin S, Lecuyer E & Hoang T Kit and Scl regulation of hematopoietic stem cells. Curr Opin Hematol 21, 256–264 (2014). [PubMed: 24857885]
17. Ali S Role of c-kit/SCF in cause and treatment of gastrointestinal stromal tumors (GIST). Gene 401, 38–45 (2007). [PubMed: 17659849]
18. Lennartsson J & Rönnstrand L Stem cell factor receptor/c-Kit: from basic science to clinical implications. Physiol Rev 92, 1619–1649 (2012). [PubMed: 23073628]
19. Ceredig R & Rolink T A positive look at double-negative thymocytes. Nat Rev Immunol 2, 888–897 (2002). [PubMed: 12415312]
20. Bluman EM et al. The c-kit ligand potentiates the allogeneic mixed lymphocyte reaction. Blood 88, 3887–3893 (1996). [PubMed: 8916954]
21. Frumento G et al. CD117 (c-Kit) is expressed during CD8. Front Immunol 10, 468 (2019). [PubMed: 30930902]
22. Falchi L & Verstovsek S Kit mutations: new insights and diagnostic value. Immunol Allergy Clin North Am 38, 411–428 (2018). [PubMed: 30007460]
23. Raghav PK, Singh AK & Gangenahalli G A change in structural integrity of c-Kit mutant D816V causes constitutive signaling. Mutat Res 808, 28–38 (2018). [PubMed: 29482074]
24. Hirota S et al. Gain-of-function mutations of c-kit in human gastrointestinal stromal tumors. Science 279, 577–580 (1998). [PubMed: 9438854]
25. Longley BJ et al. Somatic c-KIT activating mutation in urticaria pigmentosa and aggressive mastocytosis: establishment of clonality in a human mast cell neoplasm. Nat Genet 12, 312–314 (1996). [PubMed: 8589724]
26. Beghini A et al. C-kit mutations in core binding factor leukemias. Blood 95, 726–727 (2000). [PubMed: 10660321]
27. Jawhar M et al. Molecular profiling of myeloid progenitor cells in multi-mutated advanced systemic mastocytosis identifies KIT D816V as a distinct and late event. Leukemia 29, 1115–1122 (2015). [PubMed: 25567135]
28. Abbaspour Babaei M, Kamalidehghan B, Saleem M, Huri HZ & Ahmadipour F Receptor tyrosine kinase (c-Kit) inhibitors: a potential therapeutic target in cancer cells. Drug Des Devel Ther 10, 2443–2459 (2016).
29. Omori I et al. D816V mutation in the KIT gene activation loop has greater cell-proliferative and anti-apoptotic ability than N822K mutation in core-binding factor acute myeloid leukemia. Exp Hematol 52, 56–64 e54 (2017). [PubMed: 28506695]
30. Orfao A, Garcia-Montero AC, Sanchez L, Escribano L & Rema Recent advances in the understanding of mastocytosis: the role of KIT mutations. Br J Haematol 138, 12–30 (2007). [PubMed: 17555444]
31. Xiang Z, Kreisel F, Cain J, Colson A & Tomasson MH Neoplasia driven by mutant c-KIT is mediated by intracellular, not plasma membrane, receptor signaling. Mol Cell Biol 27, 267–282 (2007). [PubMed: 17060458]

32. Chaix A et al. Mechanisms of STAT protein activation by oncogenic KIT mutants in neoplastic mast cells. J Biol Chem 286, 5956–5966 (2011). [PubMed: 21135090]
33. Harir N et al. Oncogenic Kit controls neoplastic mast cell growth through a Stat5/PI3-kinase signaling cascade. Blood 112, 2463–2473 (2008). [PubMed: 18579792]
34. Larrue C et al. Oncogenic KIT mutations induce STAT3-dependent autophagy to support cell proliferation in acute myeloid leukemia. Oncogenesis 8, 39 (2019). [PubMed: 31311917]
35. Wang H et al. The proto-oncogene c-Kit inhibits tumor growth by behaving as a dependence receptor. Mol Cell 72, 413–425.e415 (2018). [PubMed: 30293784]
36. Adusumilli PS et al. Regional delivery of mesothelin-targeted CAR T cell therapy generates potent and long-lasting CD4-dependent tumor immunity. Sci Transl Med 6, 261ra151 (2014).
37. Cherkassky L et al. Human CAR T cells with cell-intrinsic PD-1 checkpoint blockade resist tumor-mediated inhibition. J Clin Invest 126, 3130–3144 (2016). [PubMed: 27454297]
38. Adusumilli PS et al. A phase I trial of regional mesothelin-targeted CAR T-cell therapy in patients with malignant pleural disease, in combination with the anti-PD-1 agent pembrolizumab. Cancer Discov 11, 2748–2763 (2021). [PubMed: 34266984]
39. Ghosn M et al. Image-guided interventional radiological delivery of chimeric antigen receptor (CAR) T cells for pleural malignancies in a phase I/II clinical trial. Lung Cancer 165, 1–9 (2022). [PubMed: 35045358]
40. Cherkassky L, Hou Z, Amador-Molina A & Adusumilli PS Regional CAR T cell therapy: An ignition key for systemic immunity in solid tumors. Cancer Cell 40, 569–574 (2022). [PubMed: 35487216]
41. Nicolet BP et al. CD29 identifies IFN-γ-producing human CD8. Proc Natl Acad Sci U S A 117, 6686–6696 (2020). [PubMed: 32161126]
42. Bhat P, Leggatt G, Waterhouse N & Frazer IH Interferon-γ derived from cytotoxic lymphocytes directly enhances their motility and cytotoxicity. Cell Death Dis 8, e2836 (2017). [PubMed: 28569770]
43. Smith KA Interleukin-2: inception, impact, and implications. Science 240, 1169–1176 (1988). [PubMed: 3131876]
44. Linnekin D Early signaling pathways activated by c-Kit in hematopoietic cells. Int J Biochem Cell Biol 31, 1053–1074 (1999). [PubMed: 10582339]
45. Xu Y et al. Closely related T-memory stem cells correlate with in vivo expansion of CAR.CD19-T cells and are preserved by IL-7 and IL-15. Blood 123, 3750–3759 (2014). [PubMed: 24782509]
46. Gattinoni L et al. A human memory T cell subset with stem cell-like properties. Nat Med 17, 1290–1297 (2011). [PubMed: 21926977]
47. Ulloa L, Doody J & Massagué J Inhibition of transforming growth factor-beta/SMAD signalling by the interferon-gamma/STAT pathway. Nature 397, 710–713 (1999). [PubMed: 10067896]
48. Kuga H et al. Interferon-gamma suppresses transforming growth factor-beta-induced invasion of gastric carcinoma cells through cross-talk of Smad pathway in a three-dimensional culture model. Oncogene 22, 7838–7847 (2003). [PubMed: 14586410]
49. Koh J et al. Regulatory (FoxP3(+)) T cells and TGF-beta predict the response to anti-PD-1 immunotherapy in patients with non-small cell lung cancer. Sci Rep 10, 18994 (2020). [PubMed: 33149213]
50. Hasegawa Y et al. Transforming growth factor-beta1 level correlates with angiogenesis, tumor progression, and prognosis in patients with nonsmall cell lung carcinoma. Cancer 91, 964–971 (2001). [PubMed: 11251948]
51. Jakubowska K, Naumnik W, Niklinska W & Chyczewska E Clinical significance of HMGB-1 and TGF-beta level in serum and BALF of advanced non-small cell lung cancer. Adv Exp Med Biol 852, 49–58 (2015). [PubMed: 25753556]
52. Urso L et al. Detection of circulating immunosuppressive cytokines in malignant pleural mesothelioma patients for prognostic stratification. Cytokine 146, 155622 (2021). [PubMed: 34153874]
53. Stockhammer P et al. Detection of TGF-beta in pleural effusions for diagnosis and prognostic stratification of malignant pleural mesothelioma. Lung Cancer 139, 124–132 (2020). [PubMed: 31778960]

54. Majzner RG et al. Tuning the antigen density requirement for CAR T-cell activity. Cancer Discov 10, 702–723 (2020). [PubMed: 32193224]
55. Feng Y et al. A novel human monoclonal antibody that binds with high affinity to mesothelin-expressing cells and kills them by antibody-dependent cell-mediated cytotoxicity. Mol Cancer Ther 8, 1113–1118 (2009). [PubMed: 19417159]
56. Chen J et al. NR4A transcription factors limit CAR T cell function in solid tumours. Nature 567, 530–534 (2019). [PubMed: 30814732]
57. Lynn RC et al. c-Jun overexpression in CAR T cells induces exhaustion resistance. Nature 576, 293–300 (2019). [PubMed: 31802004]
58. Tripathi SK et al. Genome-wide analysis of STAT3-mediated transcription during early human Th17 cell differentiation. Cell Rep 19, 1888–1901 (2017). [PubMed: 28564606]
59. Seo H et al. BATF and IRF4 cooperate to counter exhaustion in tumor-infiltrating CAR T cells. Nat Immunol 22, 983–995 (2021). [PubMed: 34282330]
60. Fucà G, Reppel L, Landoni E, Savoldo B & Dotti G Enhancing chimeric antigen receptor T-cell efficacy in solid tumors. Clin Cancer Res 26, 2444–2451 (2020). [PubMed: 32015021]
61. Foster BM, Zaidi D, Young TR, Mobley ME & Kerr BA CD117/c-kit in cancer stem cell-mediated progression and therapeutic resistance. Biomedicines 6, 31 (2018). [PubMed: 29518044]
62. Pistillo MP et al. IFN-gamma upregulates membranous and soluble PD-L1 in mesothelioma cells: potential implications for the clinical response to PD-1/PD-L1 blockade. Cell Mol Immunol 17, 410–411 (2020). [PubMed: 31217525]
63. Chen N, Li X, Chintala NK, Tano ZE & Adusumilli PS Driving CARs on the uneven road of antigen heterogeneity in solid tumors. Curr Opin Immunol 51, 103–110 (2018). [PubMed: 29554494]
64. Morello A, Sadelain M & Adusumilli PS Mesothelin-targeted CARs: driving T cells to solid tumors. Cancer Discov 6, 133–146 (2016). [PubMed: 26503962]
65. Ferrao P, Gonda TJ & Ashman LK Expression of constitutively activated human c-Kit in Myb transformed early myeloid cells leads to factor independence, histiocytic differentiation, and tumorigenicity. Blood 90, 4539–4552 (1997). [PubMed: 9373265]
66. Sepulveda H, Cerwenka A, Morgan T & Dutton RW CD28, IL-2-independent costimulatory pathways for CD8 T lymphocyte activation. J Immunol 163, 1133–1142 (1999). [PubMed: 10415007]
67. Matos ME et al. Expression of a functional c-kit receptor on a subset of natural killer cells. J Exp Med 178, 1079–1084 (1993). [PubMed: 7688785]
68. Poli A et al. CD56bright natural killer (NK) cells: an important NK cell subset. Immunology 126, 458–465 (2009). [PubMed: 19278419]
69. Gong MC et al. Cancer patient T cells genetically targeted to prostate-specific membrane antigen specifically lyse prostate cancer cells and release cytokines in response to prostate-specific membrane antigen. Neoplasia 1, 123–127 (1999). [PubMed: 10933046]
70. Krutzik PO & Nolan GP Intracellular phospho-protein staining techniques for flow cytometry: monitoring single cell signaling events. Cytometry A 55, 61–70 (2003). [PubMed: 14505311]
71. Dobin A et al. STAR: ultrafast universal RNA-seq aligner. Bioinformatics 29, 15–21 (2013). [PubMed: 23104886]
72. Engström PG et al. Systematic evaluation of spliced alignment programs for RNA-seq data. Nat Methods 10, 1185–1191 (2013). [PubMed: 24185836]

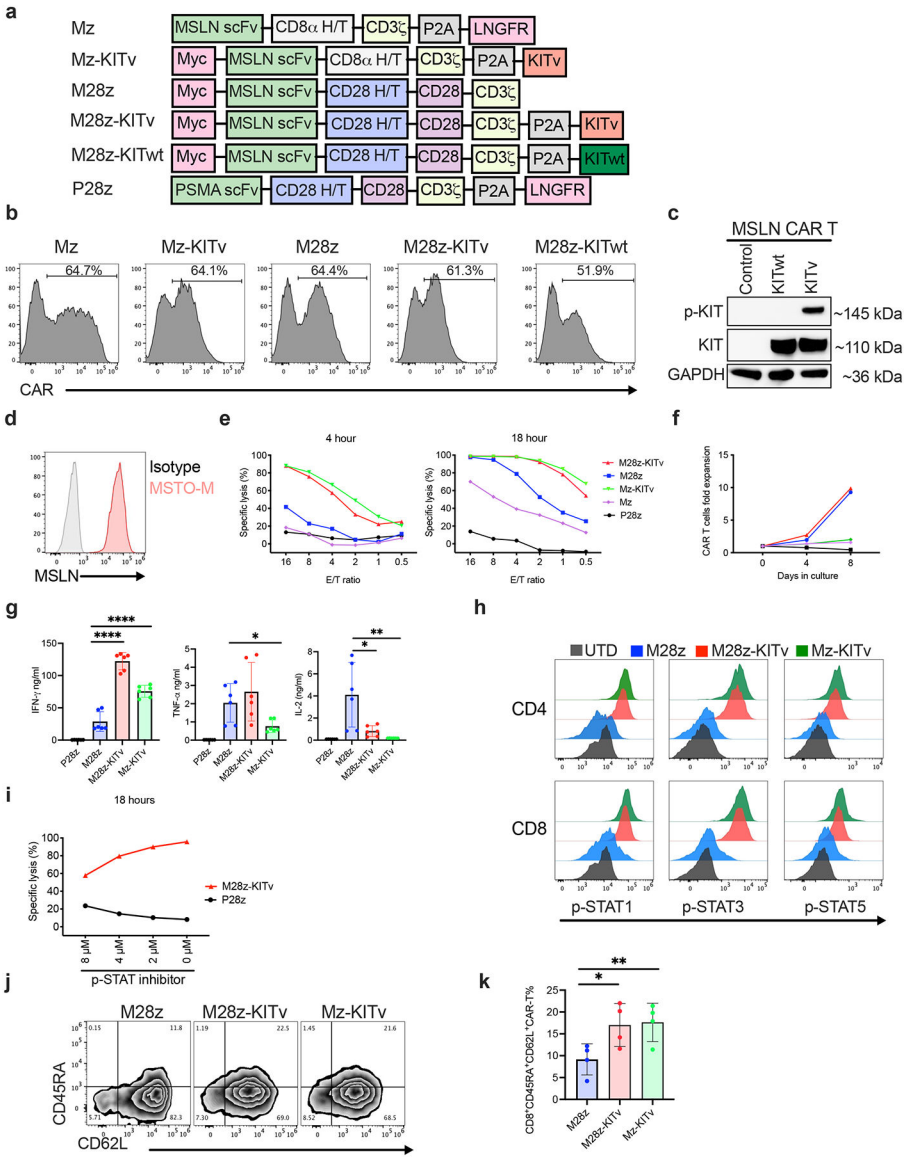

Fig. 1: KITv CAR T cells demonstrate constitutive STAT phosphorylation and higher antigen-specific target-cell lysis *in vitro*.

a, Schematic of the retroviral vector (SFG) encoding CARs targeting mesothelin (MSLN) or prostate-specific membrane antigen (PSMA), linked with or without an intracellular fragment of c-Kit or c-Kit D816V (KITwt or KITv). A c-myc-tag or ΔLNGFR is included for the detection of CARs. **b**, Representative flow cytometry histogram plots of transduced T cells, showing percentage of CAR expression. **c**, Western blot of phosphorylated (p-KIT) and unphosphorylated (KIT) c-Kit level in KITv CAR T-cell lysates. GAPDH is used as loading control. M28z and M28z CAR T cells transduced with wild-type c-KIT (KITwt) served as controls. **d**, MSLN expression level of MSTO-M (mesothelioma) cells by flow cytometry. **e**, Specific lysis of ffLuc-expressing MSLN^{+} target cells by indicated CAR T cells from luciferase-based cytotoxicity assay performed at 4 and 18 h (n=3 technical replicates; data representative of six independent experiments performed with two independent donors). **f**, Cumulative cell counts of indicated CAR T cells upon stimulation

with MSLN$^+$ target cells every 4 days (n=3 technical replicates; data representative of three independent experiments). **g**, After 18 h of coculture of respective CAR T cells with antigen (MSLN)–expressing target cells, released IFN-γ, TNF-α, and IL-2 as measured by Luminex assay are shown (n=6; three biological replicates with two technical replicates each; two-tailed unpaired *t* test ****p<0.0001, *p=0.0178, *p=0.02, **p=0.008). **h**, Comparative flow cytometric plot, showing the expression of p-STAT1, p-STAT3, and p-STAT5 in CD4$^+$ and CD8$^+$ CAR T cells. Untransduced (UTD) and M28z CAR T cells serve as controls. **i**, Specific lysis of ffLuc-expressing MSLN$^+$ target cells by M28z KITv CAR T cells in the presence or absence of STAT 3/5 inhibitor after 18 h of coculture (n=3 technical replicates; data representative of two independent experiments). **j**, Representative flow cytometry density plots showing expression of CD45RA and CD62L in indicated CAR T cells. **k**, Relative frequency of memory (CD45RA$^+$CD62L$^+$) in CD8$^+$ CAR T cells (n=4 independent donors; two-tailed paired *t* test *p=0.0346, **p=0.0060). Data are shown as mean or mean ± standard deviation.

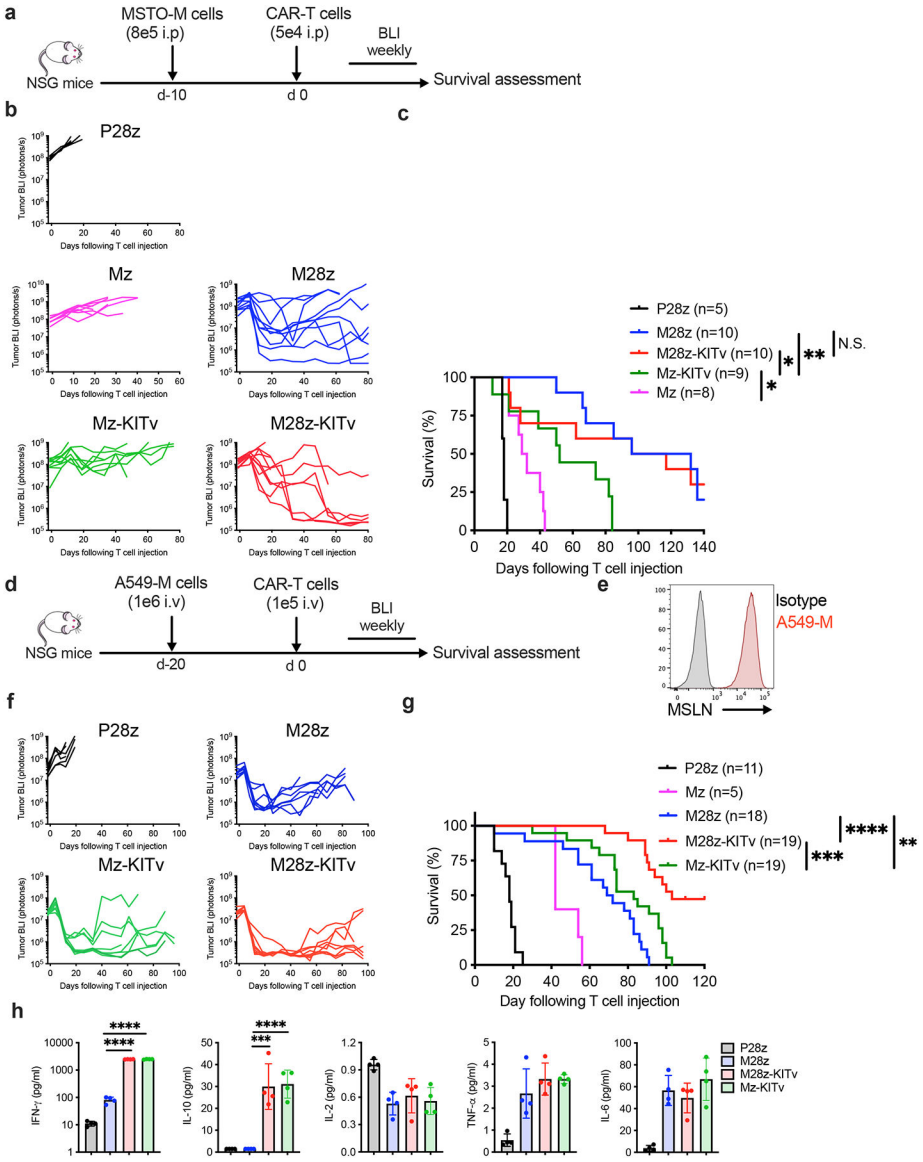

Fig. 2: KITv CAR T cells show potent antitumor efficacy in mesothelioma and lung cancer models *in vivo*.

a-c, Orthotopic pleural mesothelioma–bearing mice were treated with CAR T cells. **a**, Schematic of the orthotopic pleural mesothelioma CAR T-cell therapy. Pleural mesothelioma was established by intrapleural (i.p) administration of mesothelin (MSLN)–expressing cancer cells (8×10^5). At 10 days after establishment of tumor, cohorts of mice with equivalent tumor burden were treated with a single dose (5×10^4) of respective CAR T cells (i.p). **b**, Kinetics of tumor growth tracked by bioluminescence imaging (BLI) after CAR T-cell treatment (P28z, n=6; M28z and M28z-KITv, n=10 each; Mz-KITv, n=9; Mz, n=8 mice per cohort). **c**, Kaplan-Meier survival analysis of data shown in **b**. Data analysis was performed using a one-sided log-rank Mantel-Cox test; *p=0.0144, Mz-KITv vs. Mz; *p=0.029, M28z-KITv vs. Mz-KITv; **p=0.0028, M28z-KITv vs. Mz; N.S. p=0.5947, M28z vs. M28z-KITv. **d-g**, Metastatic lung cancer xenograft–bearing mice were treated with MSLN-targeted CAR T cells. **d**, Schematic of the metastatic lung cancer xenograft

model treated with CAR T cells intravenously (i.v). Antigen (MSLN)–expressing A549-M cancer cells (1×10^6) were administered by tail-vein injection. At 20 days after establishment of tumor, cohorts of mice with equivalent tumor burden were treated with a single dose (1×10^5) of respective CAR T cells (i.v). **e**, MSLN overexpression by A549-M cells demonstrated by flow cytometry. **f**, kinetics of tumor growth tracked by BLI after CAR T-cell treatment (n=6 mice for the P28z group, n=8 mice per group for the other groups). **g**, Kaplan-Meier survival analysis of data shown in **f**. Data analysis was performed using a one-sided log-rank Mantel-Cox test; ** p=0.009, M28z vs. Mz-KITv; *** p=0.0003, M28z-KITv vs. Mz-KITv; **** p<0.0001, M28z vs. M28z-KITv. **h**, Plasma cytokine levels from mice at day 10 after CAR T-cell infusion (n=4 mice per group). Data displayed as mean ± standard deviation and statistical analysis determined by one-way ANOVA; *** p=0.0001, **** p<0.0001. Data shown in **b** and **f** are representative of three independently repeated experiments with at least three independent donors.

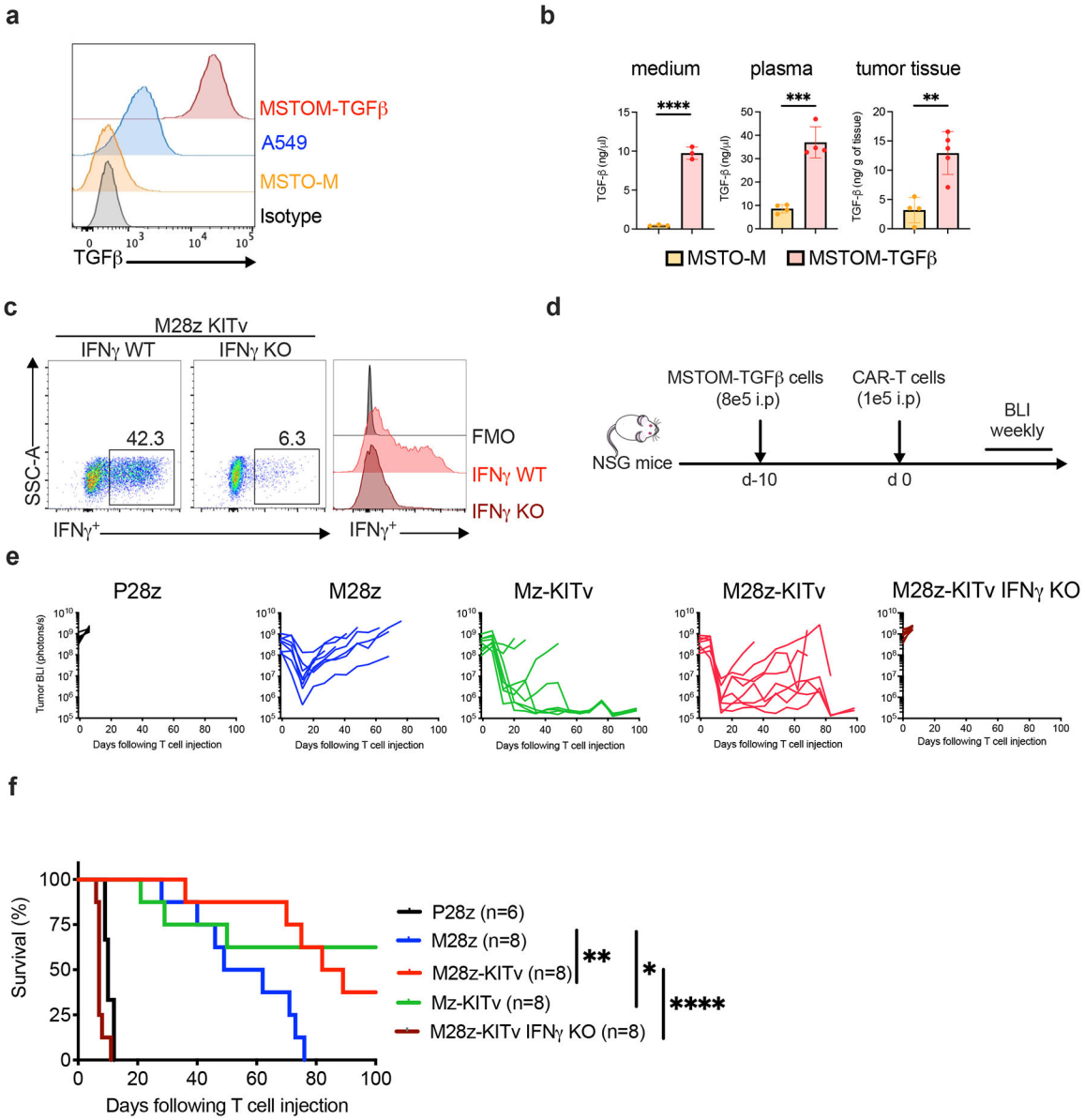

Fig. 3: KITv costimulation enhances the antitumor activity of CAR T cells in a TGF-β–rich tumor microenvironment.

a-f, Mice with orthotopic pleural mesothelioma tumor overexpressing TGF-β treated with CAR T cells. **a**, TGF-β expression level as measured by flow cytometry in lung cancer (A549) and mesothelioma (MSTO-M and MSTOM-TGFβ) cells. **b**, TGF-β protein levels in culture medium (n=3 technical replicates), plasma (n=4 biological replicates), or tumor tissue (n=4 tumors for MSTO-M and n=5 tumors for MSTOM-TGFβ group) collected from mice with equivalent tumor burden. Data shown are mean ± standard deviation, and analysis was performed using a two-tailed unpaired *t* test; ****$p<0.0001$, ***$p=0.0002$, **$p=0.0023$. **c**, Representative flow cytometric plot showing the expression of IFN-γ in IFNγ wild-type (WT) and IFNγ knock-out (KO) M28z-KITv CAR T cells after 18 h of coculture with antigen-expressing MSTO-M target cells. **d**, Schematic of the TGF-β–overexpressing mesothelioma CAR T-cell therapy. At 10 days after establishment of orthotopic pleural

mesothelioma with MSTOM-TGFβ cells, cohorts of mice with equivalent tumor burden were treated with a single dose (1×10^5) of respective CAR T cells intrapleurally (i.p). **e**, Kinetics of tumor growth tracked by bioluminescence imaging (BLI) after CAR T-cell treatment (n=6 mice for the P28z group, n=8 mice per group for the other groups). **f**, Kaplan-Meier analysis of data shown in **e**. Data analysis was performed using a one-sided log-rank Mantel-Cox test; ** p=0.0075, M28z vs. M28z-KITv; * p=0.039, M28z vs. Mz-KITv; **** p<0.0001, M28z-KITv vs M28z-KITv IFNγ KO. Data shown are representative of three independently repeated experiments with three independent donors.

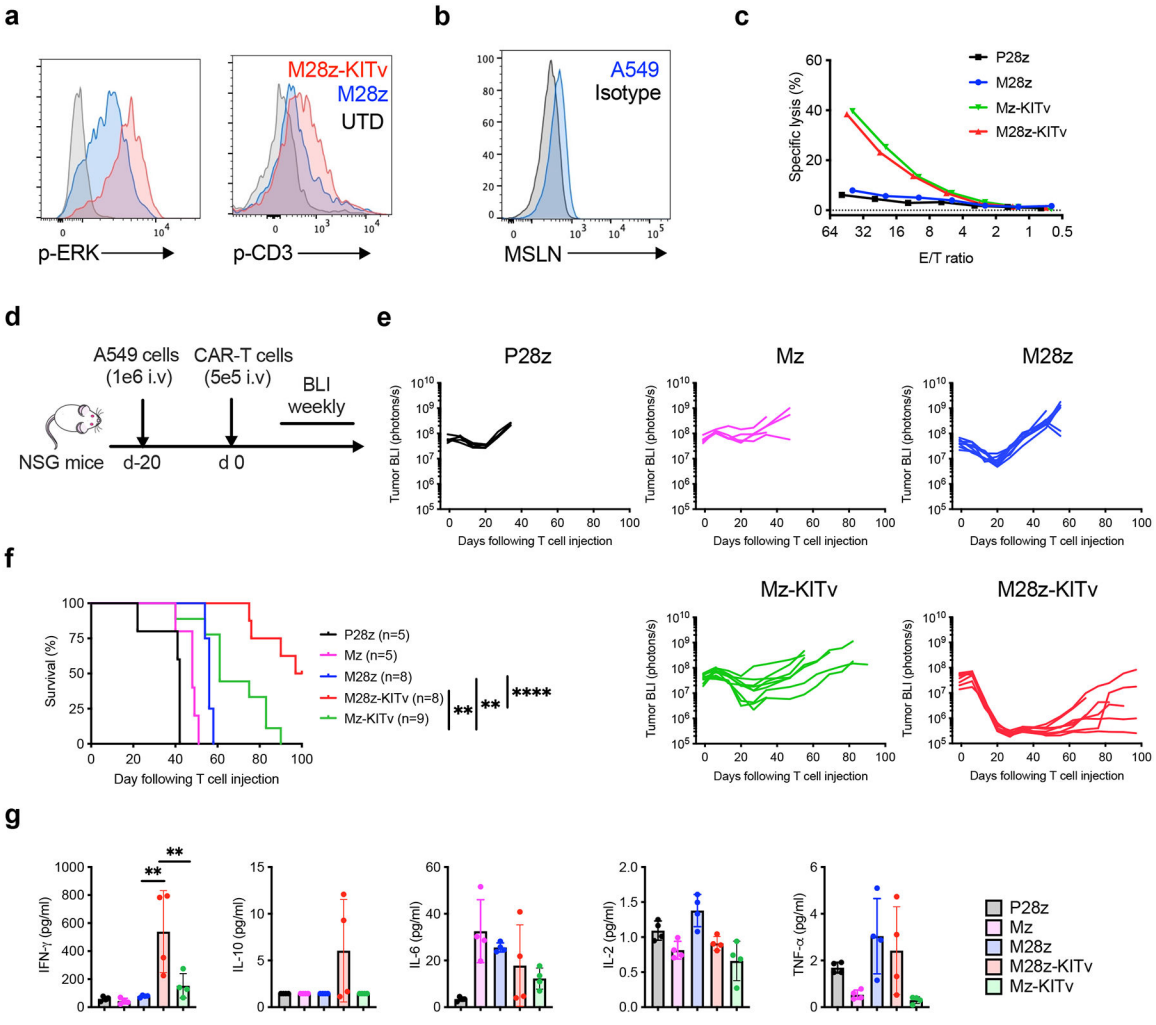

Fig. 4: KITv potentiates the antitumor efficacy of CAR T cells against low-antigen (MSLN+) lung cancer targets.

a, M28z and M28z-KITv CAR T cells were stimulated by coculture with mesothelin (MSLN)–expressing target cells for 5 min, and p-ERK and p-CD3ζ levels were measured by flow cytometry. **b**, MSLN-expression level of A549 cells measured by flow cytometry. **c**, ^{51}Cr-release cytotoxicity assay of CAR T cells. Low-antigen-expressing A549 target cells were labelled with ^{51}Cr and cocultured with respective CAR T cells at multiple E:T ratios. Cytotoxicity at 18 h was measured by ^{51}Cr-release (n=3 technical replicates; data representative of six independent experiments performed with three independent donors). **d-g**, Low-antigen-expressing A549 tumor–bearing mice were treated with CAR T cells. **d**, Schematic of the metastatic lung cancer xenograft model treated with CAR T cells. At 20 days after establishment of tumor, mice were treated intravenously (i.v) with a single dose (5×10^5) of CAR T cells. **e**, Kinetics of tumor growth tracked by bioluminescence imaging (BLI) after CAR T-cell treatment (P28z and Mz, n=5; M28z and M28z-KITv, n=8 each; Mz-KITv, n=9; mice were selected and sorted into cohorts with equivalent tumor burden as determined by BLI). **f**, Kaplan-Meier survival analysis of data shown in **e**. Data analysis was performed using a one-sided log-rank Mantel-Cox test; $^{**}p$=0.0024, M28z-

KITv vs. Mz-KITv; **p=0.0074, M28z vs. Mz-KITv; ****p<0.0001, M28z vs. M28z-KITv. **g**, Plasma cytokine levels of mice at day 10 after CAR T-cell infusion (n=4 mice per group). Data shown are mean ± standard deviation and analyzed by one-way ANOVA (**p=0.002, M28z vs. M28z-KITv; **p=0.009, M28z-KITv vs. Mz-KITv). Data shown in **e** and **g** are representative of three independently repeated experiments with at least two independent donors.

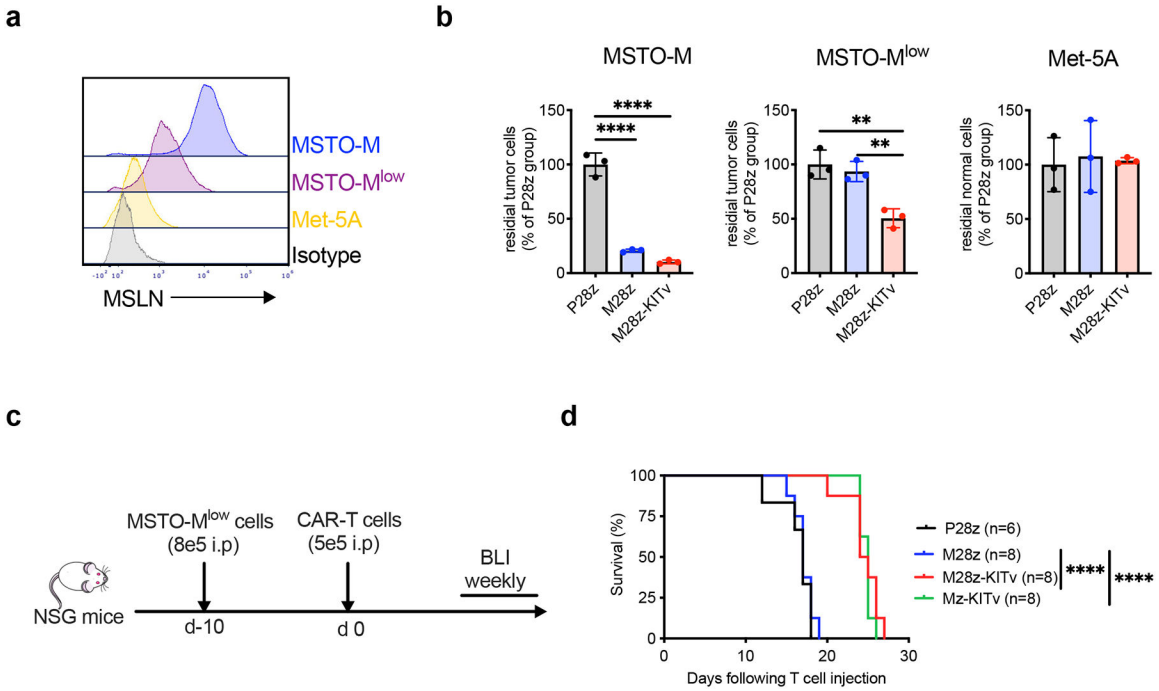

Fig. 5: KITv potentiates the antitumor efficacy of CAR T cells against low-antigen (MSLN^{+}) mesothelioma cancer targets, without cytotoxicity against mesothelial cells.

a, MSLN-expression level of MSTO-M cells (high antigen), MSTO-M^{low} cells (low antigen), or human pleural mesothelial Met5A cells (very low antigen) as measured by flow cytometry. **b**, Control nonantigen-targeted P28z, antigen-targeted M28z, and M28z-KITv CAR T cells were cocultured with MSTO-M, MSTO-M^{low}, or Met5A cells for 48 h. Target cell viability was monitored by flow cytometry (n=3 technical replicates). Data shown are mean ± standard deviation, and analysis was performed using one-way ANOVA; ****p<0.0001, MSTO-M; **p=0.0031, MSTO-M^{low} P28z vs. M28z-KITv; **p=0.0062, MSTO-M^{low} M28z vs. M28z-KITv. **c**, Schematic of the orthotopic pleural mesothelioma model. Mice were established with intrapleural (i.p) administration of MSTO-M^{low} (8×10^5) cells. At 10 days after establishment of tumor, mice were treated with a single dose (5×10^5) of CAR T cells administered intrapleurally (i.p). **d**, Kaplan-Meier analysis of survival of mice. Data analysis was performed using a one-sided log-rank Mantel-Cox test (****p<0.0001). Data shown in **b** and **d** are representative of two independently repeated experiments.

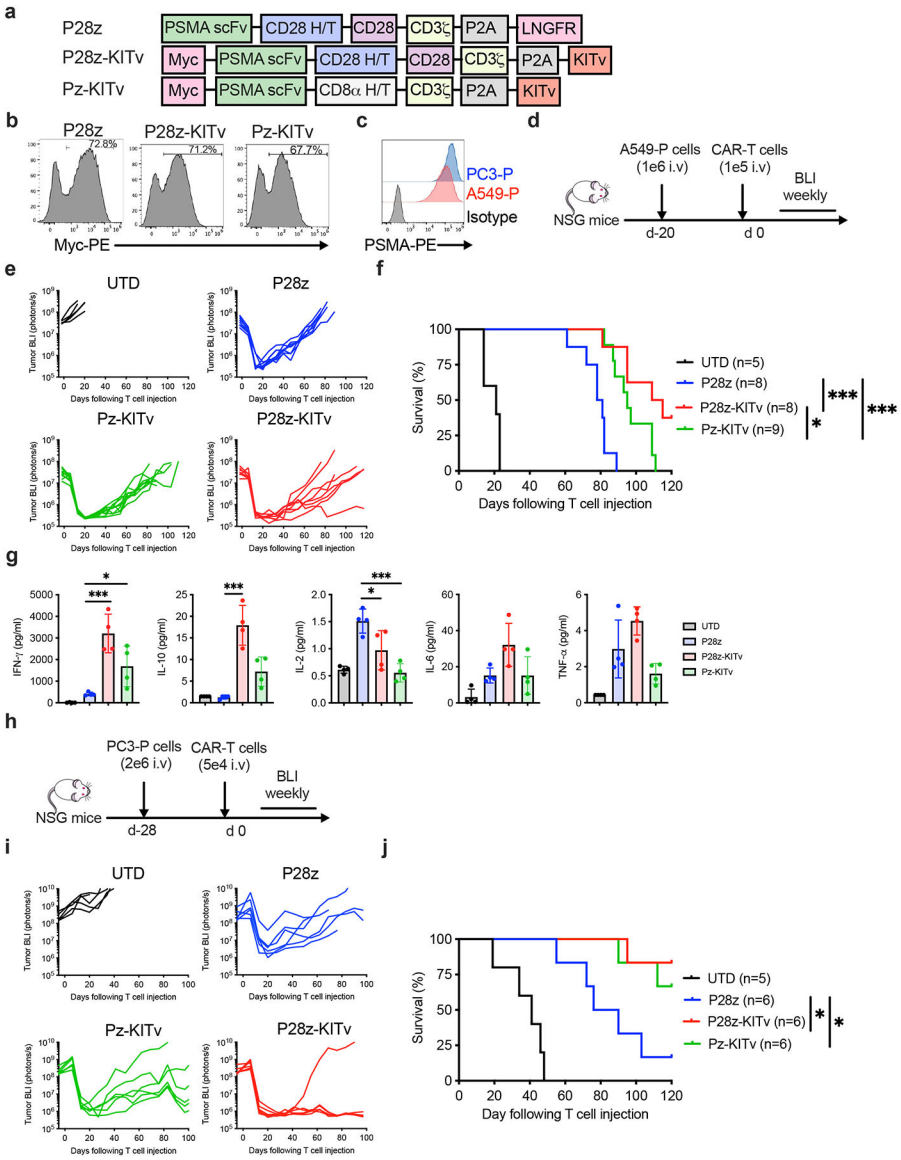

Fig. 6: KITv enhances the antitumor efficacy of prostate-specific membrane antigen (PSMA)–targeting CAR T cells.

a, Schematic of the retroviral vector (SFG) encoding CARs targeting PSMA, with CD28 costimulatory domain linked with LNGFR (P28z) or KITv (P28z-KITv) and a first-generation CAR targeting PSMA linked with KITv (Pz-KITv). A c-myc-tag is included for the detection of CARs. **b**, Representative flow cytometry histogram plots of transduced T cells, showing percentage of CAR expression. **c**, PSMA-expression levels of A549-P and PC3-P cells were measured by flow cytometry. **d-g**, A549-P tumor–bearing mice were treated with CAR T cells. **d**, Schematic of the metastatic cancer xenograft model treated with CAR T cells intravenously (i.v). **e**, Kinetics of tumor growth tracked by bioluminescence imaging (BLI) after CAR T-cell treatment (n=6 mice treated with untransduced [UTD] T cells, n=8 mice treated for the other groups; mice were selected and sorted into cohorts with equivalent tumor burden as determined by BLI). **f**, Kaplan-Meier survival analysis of data shown in **e**. Data analysis was performed using a one-sided log-rank

Mantel-Cox test; *p=0.0406, P28z-KITv vs. Pz-KITv; ***p=0.0004, P28z vs. P28z-KITv; ***p=0.0005, P28z vs. Pz-KITv. **g**, Plasma cytokine levels of mice at day 10 after T-cell infusion (n=4 mice per group). Data shown are mean ± standard deviation and analysis was performed using one-way ANOVA; *p=0.0279, IFN-γ P28z vs. Mz-KITv; ***p=0.0003, IFN-γ P28z vs. P28z-KITv; ****p<0.0001, IL-10 P28z vs. P28z-KITv; ***p=0.0004, IL-2 P28z vs. Pz-KITv; *p=0.0277, IL-2 P28z vs. P28z-KITv. **h-I**, PC3-P tumor–bearing mice were treated with untransduced or CAR T cells. **h**, Schematic of the metastatic prostate cancer xenograft model treated with CAR T cells intravenously (i.v). **i**, Kinetics of tumor BLI (n=5 mice for the P28z group, n=6 mice per group for the other groups; mice with equivalent tumor burden as determined by BLI before treatment were selected and sorted into cohorts). **j**, Kaplan-Meier survival analysis of data shown in **i**. Data analysis was performed using a one-sided log-rank Mantel-Cox test; *p=0.0169, P28z vs. P28z-KITv; *p=0.0372, P28z vs. Pz-KITv. UTD, untransduced. All data shown are representative of at least two independently repeated experiments.

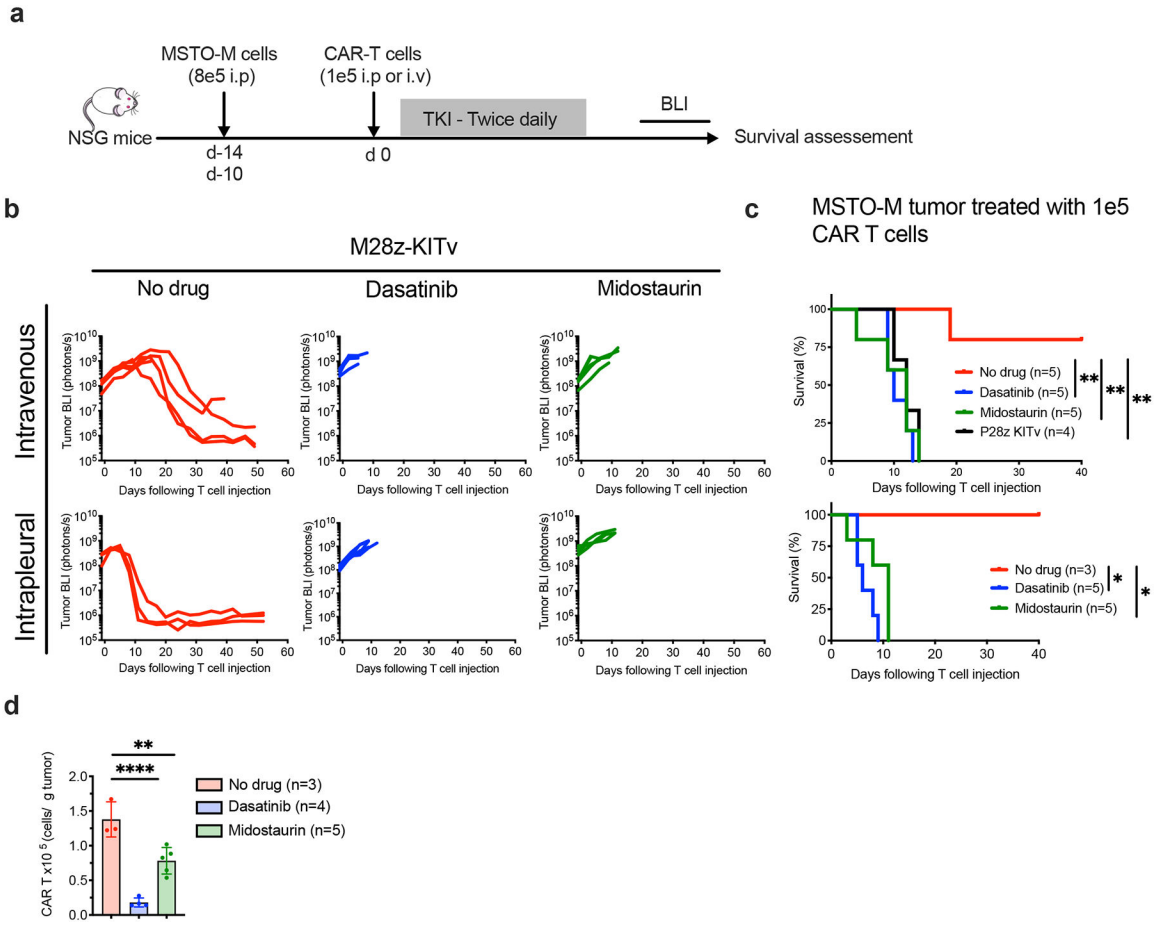

Fig. 7: M28z-KITv CAR T cells are susceptible to tyrosine kinase inhibitors (TKIs) *in vivo*.

a, Schematic of mice with orthotopic pleural mesothelioma treated with M28z-KITv CAR T cells regionally (d-14; intrapleurally [i.p]) or systemically (d-10; intravenously [i.v]), followed by daily oral administration of TKI after receiving CAR T cells. **b**, Kinetics of tumor growth tracked by bioluminescence imaging (BLI) after treatment with M28z KITv CAR T cells administered intrapleurally or intravenously. After administration of M28z-KITv CAR T cells, mice received no drug (n=3 mice) or either dasatinib or midostaurin (n=5 mice per cohort). **c**, Kaplan-Meier survival analysis of data shown in **b**. Data analysis was performed using a one-sided log-rank Mantel-Cox test; **p=0.0017, intravenous no drug vs. dasatinib; **p=0.002, intravenous no drug vs. midostaurin; **p=0.0042, intravenous no drug vs. P28z KITv; *p=0.0123, intrapleural no drug vs. dasatinib; *p=0.0169, intrapleural no drug vs. midostaurin. Data shown in **b** and **c** are representative of three independently repeated experiments with at least two donors. **d**, Flow cytometric analysis quantifying the number of CAR T cells in the harvested tumors at day 3 (n=3 tumors for no-drug group, n=4 tumors for dasatinib group, n=5 tumors for midostaurin group). Data shown are mean ± standard deviation, and analysis was performed using one-way ANOVA; ****p<0.0001, no drug vs. dasatinib; **p=0.0035, no drug vs. midostaurin.